Revision 1

Excess functions of chlorite solid solutions and neoformation of Fe-chlorites: Some implications of recent thermochemical measurements

STEPHEN AJA*

Department of Earth & Environmental Sciences,
Brooklyn College of CUNY, 2900 Bedford Avenue,
Brooklyn, NY, 11210-2889, U.S.A.

* Email address: suaja@brooklyn.cuny.edu

ABSTRACT

A full complement of standard state thermodynamic properties ($\Delta_f G^\circ_{298,1}$, $\Delta_a G^\circ_{T,i}$, $S^\circ_{298,1}$ and C°_p) has been detrmined for a magnesian chamosite [Fe-Chl(W)] and a ferroan clinochlore [Mg-Chl] investigated by calorimetry and low-temperature hydrothermal experiments; this makes these two samples the only natural chlorites whose complete set of thermochemical properties have been reported. $\Delta_f G^\circ_{298,1}$ for Mg-Chl and Fe-Chl (W) have been determined to be -8161.76±32.50 and -7278.97±21.50 kJ/mol, respectively. Ternary molecular chlorite solid solution modeling approaches have been developed for Al-rich and Si-rich chlorites; unlike available atomic site-mixing chlorite solid solution models, a molecular model obviates the need for the adoption of a *putative* structural chemistry. The calculated excess entropy of mixing in the ternary system exhibits a curvilinear dependence on composition and at 25°C, G^{ex}_{ss} vary from about -72 to 413 kJ/mol implying a significant deviation from ideality. The effect of di-trioctahedral substitutions was evaluated by modeling the solid solutions in the quaternary amesite-chamosite-clinochlore-sudoite system for aluminous chlorites; excess functions (S^{ex}, G^{ex}) calculated for these quaternary and ternary solid solutions are *marginally* different, inherently validating the ternary model. The molecular solid solution model further unmasks significant deficiencies in available database of standard state thermodynamic properties of chlorites. Finally, pursuant to the recent recognition that green rusts probably play significant roles in the cycling of iron through sedimentary sequences, the neoformation of authigenic iron chlorites from green rusts has been examined; green rusts will readily transform to berthierine and Fe-chlorites except under oxidizing conditions atypical of aquatic environments and ferrugineous sediments.

KEYWORDS: ternary chlorite solid solutions, quaternary chlorite solid solutions, green rust chlorite precursor, excess thermodynamic properties.

Introduction

Chlorites are phyllosilicates in which adjacent 2:1 talc layers are linked by an octahedral brucite sheet; their general structural formula $\left(\mathrm{R}^{2+}_{6-y-z}\mathrm{R}^{3+}_{y}\,\square_{z}\right)_2\left(\mathrm{Si}_{4-k}\mathrm{R}^{3+}_{k}\right)_2\mathrm{O}_{20}(\mathrm{OH})_{16}$ consists of alternating talc layer $\left(\mathrm{R}^{2+}_{6-y_2-z_2}\mathrm{R}^{3+}_{y_2}\,\square_{z_2}\right)\left(\mathrm{Si}^{4+}_{4-k}\mathrm{R}^{3+}_{k}\right)\mathrm{O}_{20}(\mathrm{OH})_4$ and brucite sheet $\left(\mathrm{R}^{2+}_{6-y_1-z_1}\mathrm{R}^{3+}_{y_2}\,\square_{z_1}\right)(\mathrm{OH})_{12}$ along the *c* crystallographic direction (Bailey, 1988; Zazzi et al. 2006). The extent of substitution of trivalent cations (R^{3+}) in the octahedral and tetrahedral sheets are represented by *y* (the sum of $y_1 and\ y_2$) and *k*, respectively; the total octahedral vacancy (z) is the sum of the vacancies in both octahedral sheets (z_1 and z_2) and y is the sum of y_1 and y_2. Refined atomic site occupancies have been reported in the form $(\mathrm{M1,M2})(\mathrm{M3,M4})(\mathrm{T1,\ T2})\mathrm{O}_{20}(\mathrm{OH})_{16}$; for instance, the structural formula of an ordered triclinic clinochlore was reported as (Smyth et al. 1997), on a half-unit cell basis, as

$$(\mathrm{Mg}_{0.966}\mathrm{Fe}_{0.034})^{\mathrm{M1}}(\mathrm{Mg}_{0.962}\mathrm{Fe}_{0.038})^{\mathrm{M2}}_{2}(\mathrm{Mg}_{0.996}\mathrm{Fe}_{0.004})^{\mathrm{M3}}_{2}(\mathrm{Al}_{0.841}\mathrm{Fe}^{3+}_{0.102}\mathrm{Cr}_{0.004}\mathrm{Ti}_{0.004})^{\mathrm{M4}}(\mathrm{Si}_{2.96}\mathrm{Al}_{1.04})\mathrm{O}_{10}(\mathrm{OH})_8$$

T1 and T2 describe the distinct tetrahedral sites found in the talc layer whereas the distinct octahedral sites of the talc layer are denoted as M1 and M2. M3 and M4 are the octahedral sites located in the brucite sheet though there are half as many M4 as M3 sites per layer. The two tetrahedral sites are somewhat homologous given their identical volume and average metal-oxygen bond distance and show little ordering of Al and Si between T1 and T2. The M3 and M4 octahedral sites differ significantly in octahedral volume, distortion and mean cation-oxygen bond distance. Considerable cation ordering occurs in the brucite sheet with the preference of trivalent cations for the M4 site and virtually no Fe in the M3 site (Smyth et al. 1997). Furthermore, evidence for cation ordering in the octahedral sites of the talc layer is equivocal; the preference of Al for the M1 site was inferred by Welch et al. (1995) based on ^{27}Al and ^{29}Si MAS NMR and was attributed to Al avoidance in the talc tetrahedral sheet; by contrast, the distinction between the tetrahedral sites was not confirmed in the crystallographic study of Smyth et al. (1997).

Petrogenetically, chlorites constitute a major minerals group found in a wide variety of geological environments. Authigenic chlorites are common in siliciclastic petroleum reservoirs where they may occur as pore-filling and/or grain-coating chlorites, isolated rosettes, grains-replacing microcrystalline aggregates and pore-lining crystals (Grigsby, 2001; Hillier, 1994; Bahlis and De Ros, 2013). The presence of chlorite cement (as pore-lining, pore-filling, grain coating chlorites, etc.) result in the preservation of abnormally high porosity in some petroleum reservoir sandstones; these authigenic chlorites retard the formation of quartz overgrowths (Bloch et al. 2002; Berger et al. 2009) which will be normally deleterious to overall rock porosity.

The wide range of environmental settings in which chlorite authigenesis has occurred in sedimentary formations (Bartier et al. 1998; Bloch et al. 2002; Gould et al. 2010; Dowey, 2012; Tetiker et al. 2015) suggests the existence of a chlorite stability field under these low temperature hydrothermal environments. Furthermore, the consequences of chlorite authigenesis on the petrophysical properties of siliciclastic hydrocarbon reservoirs has practical application to issues of carbon sequestration in sedimentary formation. The capture and geologic sequestration of CO_2 emitted by industrial processes has been proposed as a possible approach to mitigate anthropogenic-driven increases in the level of CO_2 in earth‘s atmosphere (Lu et al. 2012; Kampman et al. 2014; Lammers et al. 2015). Some of the geologic formations in which the carbon dioxide will be sequestered are chlorite bearing which underscores the need for a thorough definition of both the thermodynamic and kinetic aspects of chlorite stability in the low to modest temperature hydrothermal environments associated with such sedimentary formations.

The thermochemical properties of chlorites have been reported by several investigators (Kittrick, 1982; Hemingway et al. 1984; Bertoldi et al. 2001; Bertoldi et al. 2007; Gailhanou et al. 2009; Blanc et al. 2014; Ogorodova et al. 2016). Kittrick (1982) studied the solubility of four natural chlorites at 25 °C and in a latter investigation, Hemingway et al. (1984) studied two of those chlorites by calorimetry. Bertoldi et al. (2001, 2007) reported heat capacity measurements for five different chlorite samples (spanning a wide range in mole fraction of Fe). Ogorodova et al. (2016) measured the enthalpies of formation of two clinochlores using melt solution calorimetry. In a combination of heat-pulse and acid solution calorimetric techniques, Gailhanou et al. (2009) and Blanc et al. (2014) measured the properties of ISGS berthierine $[(\mathrm{Al}_{0.976}\mathrm{Fe}^{3+}_{0.182}\mathrm{Fe}^{2+}_{1.44}\mathrm{Mg}_{0.157})(\mathrm{Si}_{1.332}\mathrm{Al}_{0.668})\mathrm{O}_5(\mathrm{OH})_4,]$ and the Clay Minerals Special Clay, CCa-2, $[(\mathrm{Si}_{2.633}\mathrm{Al}_{1.367})(\mathrm{Al}_{1.116}\mathrm{Fe}^{3+}_{0.215}\mathrm{Mg}_{2.952}\mathrm{Fe}^{2+}_{1.712}\mathrm{Mn}_{0.012}\mathrm{Ca}_{0.011})\mathrm{O}_{10}(\mathrm{OH})_8]$. The combination of these approaches by Blanc et al. (2014) facilitated retrieval of a nearly complete spectrum of standard state properties for CCa-2 and ISGS berthierine. Hence, amongst the natural chlorites (circa 14 samples) whose thermodynamic properties have been reported to date, the only sample for which there is nearly a full complement of experimentally-derived standard state thermochemical properties is CCa-2; however, the contribution of configurational entropy (ΔS_{conf}) to third law entropy (S°) was not determined for CCa-2. Third law entropy encompasses the lattice dynamic contribution to entropy ($\int_0^{298.15} \frac{C_p}{T} dT$), configurational entropy owing to site mixing (ΔS_{conf}) and associated phase-change entropies arising primarily from magnetic spin ordering (ΔS_p); that is (cf. Ulbrich and Waldbaum, 1976),

$$S^{\circ} = \int_0^{298.15} \frac{C_p}{T} dT + \Delta S_{conf} + \Delta S_p$$

The contribution of magnetic spin ordering peaks at about 10 K (Aja et al. 2015) and in the absence of additional phase changes contributions, the third law entropy of chlorites thus consists of the calorimetric entropy part and contributions owing to atomic site mixing. In this study, standard state thermochemical properties are being reported for two natural chlorite samples [Fe-Chl(W) and Mg-Chl]; these data have been retrieved by combining the results of our recent calorimetric measurements and low temperature hydrothermal experiments, and increase the number of natural chlorite samples for which a full complement of standard state thermodynamic properties are available. Furthermore, a molecular chlorite solid solution model has also been developed and the possible implications of the available thermodynamic data for the neoformation of Fe chlorite have also been evaluated.

Methods

Previous Experimental Investigations

In previous experimental studies (Aja and Small, 1999; Aja and Dyar, 2002), the relative stabilities of natural Fe-Mg chlorites in low-temperature hydrothermal solutions were investigated; chlorite mixtures with kaolinite (± quartz, ± gibbsite) were equilibrated under isothermal, isobaric (25°C $\leq$ T ≤ 250 °C; $P_v = P_{H_2O}$) conditions. The experiments were designed to approach the equilibrium boundaries from both under- and super-saturation conditions; the solid products from the investigations and the starting materials were characterized by a variety of techniques including X-ray fluorescence spectroscopy (XRF), analytical transmission electron miscroscopy (ATEM), powder X-ray diffraction (XRD) and Mössbauer spectroscopy. The equilibrated solutions were analyzed for aqueous silica (by colorimetry using the silicomolybdate blue complex) and for other dissolved solutes by ICP-MS. These solution equilibration investigations demonstrated that: 1) chlorite-fluid equilibrium is attainable under the diagenetic and hydrothermal alteration conditions of the experiments; 2) the law of mass action (i.e., the solubility constant approach) is applicable to chlorite-fluid equilibria; and 3) that the slopes of phase boundaries in several different types of chemical potential diagrams are determined by the compositions of the solubility-limiting chlorite phases. Thus, under isothermal, isobaric conditions, these compositionally-complex natural chlorites were shown to behave (during the solution equilibration investigations) as single-phase, single-component micas of fixed compositions. The kaolinite-chlorite equilibrium reactions were subsequently generalized as (Aja, 2002):

$$\begin{aligned}&(\mathrm{Al}_{2.33}\mathrm{Fe}^{2+}_{1.00}\mathrm{Fe}^{3+}_{0.14}\mathrm{Ca}_{0.02}\mathrm{Mn}_{0.01}\mathrm{Ni}_{0.02}\mathrm{Cr}_{0.01}\mathrm{Mg}_{8.40}\square_{0.07})(\mathrm{Si}_{5.66}\mathrm{Al}_{2.34})\mathrm{O}_{20}(\mathrm{OH})_{16} \\ &\quad + 19.21\ \mathrm{H}^{+}_{(\mathrm{aq})} \\ &\rightleftharpoons 2.335\mathrm{Al}_2\mathrm{Si}_2\mathrm{O}_5(\mathrm{OH})_4 + 8.40\mathrm{Mg}^{2+}_{(\mathrm{aq})} + 0.02\ \mathrm{Ni}^{2+}_{(\mathrm{aq})} + 1.14\ \mathrm{Fe}^{2+}_{(\mathrm{aq})} + 0.02\ \mathrm{Ca}^{2+}_{(\mathrm{aq})} \\ &\quad + 0.01\ \mathrm{Mn}^{2+}_{(\mathrm{aq})} + 0.01\ \mathrm{Cr}^{3+}_{(\mathrm{aq})} + 0.99\ \mathrm{SiO}_{2(\mathrm{aq})} + 12.935\ \mathrm{H}_2\mathrm{O} \\ &\quad + 0.035\ \mathrm{O}_{2(\mathrm{g})} \qquad (1a)\end{aligned}$$

$$\begin{aligned}&(\mathrm{Fe}^{3+}_{0.60}\mathrm{Fe}^{2+}_{5.43}\mathrm{Mg}_{2.30}\mathrm{Al}_{2.98}\mathrm{Mn}_{0.05}\mathrm{Ca}_{0.03}\mathrm{Zn}_{0.01}\square_{0.60})(\mathrm{Si}_{5.63}\mathrm{Al}_{2.37})\mathrm{O}_{20}(\mathrm{OH})_{16} \\ &\quad + 16.83\ \mathrm{H}^{+}_{(\mathrm{aq})} \\ &\rightleftharpoons 2.675\ \mathrm{Al}_2\mathrm{Si}_2\mathrm{O}_5(\mathrm{OH})_4 + 6.03\ \mathrm{Fe}^{2+}_{(\mathrm{aq})} + 2.30\ \mathrm{Mg}^{2+}_{(\mathrm{aq})} + 0.05\ \mathrm{Mn}^{2+}_{(\mathrm{aq})} + 0.03\ \mathrm{Ca}^{2+}_{(\mathrm{aq})} \\ &\quad + 0.01\ \mathrm{Zn}^{2+}_{(\mathrm{aq})} + 0.28\ \mathrm{SiO}_{2(\mathrm{aq})} + 11.065\ \mathrm{H}_2\mathrm{O} + 0.15\ \mathrm{O}_{2(\mathrm{g})} \qquad (1b)\end{aligned}$$

Over the range of temperatures investigated (25 – 250 °C), the equilibrium constant expressions for the kaolinite – chlorite equilibrium reactions were:

$$\log \mathrm{K}_{1a} = 520.87 - \frac{14198}{\mathrm{T}} - 168.20 \log \mathrm{T} \qquad (R^2 = 0.99) \qquad (2a)$$

and

$$\log \mathrm{K}_{1b} = -49.72 + \frac{20137}{\mathrm{T}} \qquad (\mathrm{R}^2 = 0.98) \qquad (2b)$$

At 25 °C, log K was determined to be 57.45 ± 6.21 and 18.09 ± 2.24 for reactions 1a and 1b, respectively.

$\Delta_f G^{\circ}_{298,1}$, the standard state Gibbs free energy of formation, of FeChl(W) and Mg-Chl were then determined from the solution equilibration data using standard protocols (Aja, 2002); that is,

$$\Delta \mathrm{G}^{\circ}_{\mathrm{rxn}} = -2.303 RT \log K \qquad \text{(Eqn. 3a)}$$

$$\Delta_f G^{\circ}_{298,1} = -\Delta G^{\circ}_{rxn} + \sum_i \Delta_f G^{\circ}_{i,298} \qquad \text{(Eqn. 3b)}$$

$\sum_i \Delta_f G^{\circ}_{i,298}$ in Eqn. 3b sums the Gibbs free energy of formation of the species in equation 1 besides the chlorites, log K is equilibrium constant (Eqn. 2), and R is the universal gas constant (8.314 J•mol^{-1}•K^{-1}). Using Eqn. 3, the Gibbs free energy of formation for Fe-Chl(W) and MgChl are determined to be -7269.13±14.33 kJ/mol and -8182.67±32.46 kJ/mol, respectively.

For the calorimetric phase of the investigations, the chlorites were further characterized by electron probe microanalysis (EPMA) and by powder diffraction techniques using synchroton radiation techniques coupled with Rietveld analyses of the diffraction data. On a half-unit cell basis, the structural compositions of Fe-Chl (W) and Mg-Chl, were reported to be (Aja et al. 2015), $(Al_{1.48}Fe^{3+}_{0.33}Fe^{2+}_{2.73}Mg_{1.19}Mn_{0.026}Zn_{0.007}\,\square_{0.237})(Si_{2.62}Al_{1.38})O_{10}(OH)_8$ and $(Al_{1.32}Cr^{3+}_{0.003}Fe^{3+}_{0.06}Fe^{2+}_{0.49}Mg_{3.97}Ni_{0.009}\,\square_{0.148})(Si_{2.86}Al_{1.14})O_{10}(OH)_8$, respectively. The calorimetric measurements were taken with differential scanning calorimetry (DSC) and the heat capacity option of physical properties measurement system (PPMS produced by Quantum Design®). The heat capacities for the chlorite samples were measured between 2 K and 300 K using PPMS whereas using DSC, the heat capacities were measured between 282 and 764 K. The respective heat capacity polynomials for Mg-Chl and Fe-Chl(W) (280 ≤ T ≤ 570 K) were respectively reported as:

$$C_p = 1185.44(\pm 68.93) - 9753.21(\pm 2186.85)T^{-0.5} - 1.9094(\pm 1.0288) \bullet 10^{7}T^{-2} + 3.3013(\pm 1.5363) \bullet 10^{9}T^{-3}$$

and

$$C_p = 1006.06\,(\pm 48.46) - 4134.83\,(\pm 1515.16)T^{-0.5} - 40.0949(\pm 6.9413) \bullet 10^{6}T^{-2} + 5.9386(\pm 1.0287) \bullet 10^{9}\,T^{-3}$$

Thermochemical calculations

In the prior investigations, mole site occupancies of the chlorites [Mg-Chl and Fe-CHl(W)] were obtained by XRF during the hydrothermal experiments and by EPMA during the calorimetric investigations; though these are virtually identical but the apparent compositional differences are consequential in extraction of extensive thermodynamic properties. In order to place the standard state molar Gibbs free energy of formation determined using Eqn. 3 on the same compositional basis as the calorimetric data, it has been adjusted using fictive solid-solid reactions per the approach of Blanc et al. (2014) and Gailhanou et al. (2013); that is,

$$\Delta_f G^{\circ}_{\mathrm{chlorite,A}} + \sum_{i} \Delta_f G^{\circ}_{\mathrm{oxides,B}} \rightleftharpoons \Delta_f G^{\circ}_{\mathrm{chlorite,B}} + \sum_{j} \Delta_f G^{\circ}_{\mathrm{oxides,A}} \qquad (4)$$

The underlying presumption in this technique is that the Gibbs free energy of reaction for this solid-solid reaction is zero. Chlorites A and B (in Eqn. 4) designate the two slightly different chlorite compositions from XRF and EPMA whereas oxides B and A refer to the major oxide species and its equimolar trace oxide species by which chlorite A is transformed to chlorite B. $\Delta_f G^{\circ}_{298,1}$ for oxide species were obtained from Robie and Hemingway (1995).

$\Delta_a G^{\circ}_{T,i}$, the apparent standard molal Gibbs free energies of formation at saturated vapor pressures, have been calculated for the chlorites [Mg-Chl, Fe-Chl(W) and CCa-2] by means of equation 5; that is,

$$\Delta_a G^{\circ}_{T,i} = \Delta_f G^{\circ}_{298,1} - S^{\circ}_{298,1}(T - T_r) + \int_{298}^{T} C^{\circ}_{p,i}\,dT - T\int_{298}^{T} \frac{C^{\circ}_{p,i}}{T}\,dT + V^{\circ}_{1,298}(P-1) \quad \text{(Eqn. 5)}$$

For samples Mg-Chl and Fe-Chl(W), $\Delta_f G^{\circ}_{298,1}$ (in Eqn. 5) were determined from solution equilibration data (Eqns 1 - 4), heat capacity and entropy were determined by calorimetry (Aja et al. 2015); the molar volumes used in equation 5 were obtained from X-ray diffractometry (Aja et al. 2015). For chlorite CCa-2, the data source used in calculating apparent Gibbs energy were obtained from Blanc et al. (2014).

Excess entropies were calculated using Eqn. 6 (cf. Anderson and Crerar, 1993); that is,

$$\mathrm{S^{ex}} = \mathrm{S_{real}} - \mathrm{S_{ideal}} = \mathrm{S_{Chl,\,measured}} - \left(\sum\nolimits_i \mathrm{X_i S_i} - \mathrm{R}\sum\nolimits_i \mathrm{X_i} \ln \mathrm{X_i}\right) \qquad (6)$$

In Eqn. 6, $\mathrm{S_{real}}$ (i.e., $\mathrm{S_{chl,\,measured}}$) is the calorimetric entropy of natural chlorite given in Table 1 whereas $\mathrm{X_i}$ and $\mathrm{S_i}$ designate the respective molar fractions and calorimetric entropies of the endmember components defining the solid solution. In choosing entropy of endmember components (S_i, Eqn. 6), literature values for endmember phases were first compared with measured calorimetric entropies for the natural chlorites (see Figure 1) by plotting the entropies as a function of mole fraction of Fe (X_{Fe}); the latter is typically presumed to be an index of the binary clinochlore-chamosite solid solution. The measured calorimetric entropies appear to vary somewhat linearly with mole fraction of Fe and such a linear trend implies little or slightly positive excess vibrational entropy in the solid solution. Also shown in Fig. 1 are clinochlore-chamosite mixing lines presumed using the data from Holland and Powell (2011), Vidal et al. (2005) and Holland and Powell (1998); evidently, the entropy values published for chamosite and clinochlore by Holland and Powell (1998) seem more consistent with measured calorimetric entropies for the natural samples. Though the more recent endmember entropies of Holland and Powell (2011) and Vidal et al. (2005) may be indicative of large excess vibrational entropy in the chlorite solid solution, the apparent discrepancy among the datasets may also stem from the fact that entropies extracted from phase equilibrium data and from petrogenetic studies may really be third law entropies rather than calorimetric entropies. For this study, however, entropy values for the endmember phases reported by Holland and Powell (1998) have been adopted.

Excess Gibbs energy of mixing was calculated using the following expression:

$$\mathrm{G}^{\mathrm{ex}}_{\mathrm{s.s.}} = \mathrm{G}^{\circ}_{\mathrm{real}} - \left(\sum \mathrm{X_i G^{\circ}_i} - \mathrm{RT} \sum \mathrm{X_i} \ln \mathrm{X_i}\right) \tag{7}$$

In Eqn. 7, G°_{real} is the standard Gibbs free energy of formation ($\Delta_f G^{\circ}_{298,1}$) tabulated in table 2, G°_i refers to the standard state Gibbs free energy of formation of the endmember components (obtained from Holland and Powell, 1998) and X_i is the mole fraction of the endmember components.

Results

Thermodynamic Properties

Values of $\Delta_f G^{\circ}_{298,1}$ for Mg-Chl and Fe-Chl(W) adjusted using Eqn. 5 are given in Table 2 and these lie within the 1σ confidence interval of the value based on the experimental solution equilibration data (i.e., from Eqns 1-3). Table 2 also shows values of $\Delta_f G^{\circ}_{298,1}$ reported recently for CCa-2 (Blanc et al., 2014) and calculated values of $\Delta_a G^{\circ}_{T,i}$ for CCa-2, Fe-Chl(W) and Mg-Chl using Eqn. 5. The uncertainty in the Gibbs free energy of formation reported for the two chlorites in this study (0.30 to 0.40 %) is much larger than that reported for CCa-2 (0.11%). This difference is rooted in the experimental techniques; acid solution calorimetry is somewhat more precise being focused on measuring the heat content of a single phase though it cannot directly provide levels of solute activites in hydrothermal solutions at equilibrium with the phase. Solution equilibration, on the other hand, directly furnishes this knowledge but is subject to experimental constraints inherent in the determination of phase boundaries; that is, the normal asymptotic decrease of free energy of reactions as an equilibrium boundary is approached is exarcerbated by the mechanistic complexities of coupled hydrolytic reactions (i.e. Eqn. 1).

The apparent free energies of formation, $\Delta_a G^{\circ}_{T,i}$, have been depicted as an inverse function of temperature (Fig. 2). Despite the use of different experimental techniques in extracting the thermodynamic properties, the variation of $\Delta_a G^{\circ}_{T,i}$ with inverse temperature reflect the compositions of the chlorites as is expected, and as previously noted, $\Delta_f G^{\circ}_{298,1}$ for CCa-2 was determined by acid solution calorimetry whereas for Mg-Chl and Fe-Chl (W), $\Delta_f G^{\circ}_{298,1}$ was obtained from solution equilibration experiments. Furthermore, the shallowness of the G – T sections, over the temperature range studied, suggests that some reactions involving chlorite are likely to be characterized by small changes in entropy; dehydroxylation reactions appear to occur at higher temperatures (T ≈ 600 K; see Aja et al. 2015) which certainly will affect the entropy of chlorite-bearing reactions.

Discussions

A Molecular Approach to Chlorite Solid Solutions

Chlorite solid solution models proposed heretofore have included a regular-solution site-mixing model, ideal site mixing models in which cation distribution is presumed to be random on energetically-equivalent sites and mixing of atoms on energetically-distinct structural sites (Stoessell, 1984; Helgeson and Aagaard, 1985; Holland et al., 1998). Stoessell (1984) developed a random, regular-solution site-mixing model based on a set of six end-member component phases [amesite $(Mg_4Al_2)(Si_2Al_2)O_{10}(OH)_8$, chamosite $(Fe_4^{2+}Al_2)(Si_2Al_2)O_{10}(OH)_8$, Fe^{3+}- chamosite $(Fe_4^{2+}Fe_2^{3+})(Si_2Al_2)O_{10}(OH)_8$, talc-3 brucite $(Mg_6)(Si_4)O_{10}(OH)_8$, minnesotaite-3 $Fe(OH)_2[(Fe_6^{2+})(Si_4)O_{10}(OH)_8$, pyrophyllite-2 gibbsite $(Al_4)(Si_4)O_{10}(OH)_8$]; some of these end-members were fictive 14 Å chlorites whose thermochemical properties were unknown. Holland et al. (1998) proposed a fictive solid solution model between Al-free chlorite [$Mg_6Si_4O_{10}(OH)_8$], clinochlore [$(Mg_5Al)(Si_3Al)O_{10}(OH)_8$], amesite [$(Mg_4Al_2)(Si_2Al_2)O_{10}(OH)_8$] and chamosite [$(Fe_5^{2+}Al)(Si_3Al)O_{10}(OH)_8$]. They presumed a strong ordering of octahedral Al into the M4 site though Al enters into both the M1 and M4 sites, and that random substitution of tetrahedral Al for Si occurs only on the T2 sites; furthermore, they presumed a rather simple chlorite chemistry [$(R_{6-x}^{2+}Al_x)(Si_{4-x}Al_x)O_{10}(OH)_8$] and the absence of octahedral vacancies in the 2:1 layer. The model incorporates ideal configuring entropy arising from partition between M1 and M4 sites coupled with a regular solution for the enthalpic part of mixing of the atoms. They also employed an order parameter and a compositional parameter to define the activity of each endmember in the solid solution. For instance, the ideal part of the activity of endmember clinochlore in the solid solution was given (Holland et al. 1998) by

$$a_{\mathrm{Clc}}^{\mathrm{ideal}} = 4X_{\mathrm{Mg}}^{\mathrm{M1}}X_{\mathrm{Al}}^{\mathrm{M4}}X_{\mathrm{Si}}^{\mathrm{T2}}X_{\mathrm{Al}}^{\mathrm{T2}} = 4(1-y+N)(y+N)(1-y)y$$

whereas the non-ideal part expressed through the activity coefficient, γ, was

$$\mathrm{RT}\ln\gamma_{\mathrm{clc}} = -p_{\mathrm{Afchl}}p_{\mathrm{Ame}}W_{\mathrm{Af,Ame}} + p_{\mathrm{Afchl}}(1-p_{\mathrm{Clc}})W_{\mathrm{Afchl,Clc}} + p_{\mathrm{Ame}}(1-p_{\mathrm{Clc}})W_{\mathrm{Clc,Ame}}$$

In the expressions above, *y* is the compositional parameter, *p* pertains to the molar proportions of the endmember. The model proposed by Holland et al. (1998) was in an effort to harmonize predicted and experimental compositional dependence on temperature for the chlorite + forsterite + orthopyroxene assemblage under elevated P-T conditions. Vidal et al (2001) sought to extend the model of Holland et al. (1998) with the proviso that octahedral vacancies in chlorites, omitted in the prior model, formed at temperatures < 450 °C are not artifacts of mixed layering; they therefore proposed a 3-site mixing model having symmetric Margules parameters and ideal inter-site interaction. The revised model is applicable to a wider P-T range and presumes that octahedral vacancies result from di-trioctahedral substitutions, that all Fe is divalent, and that compositional variation in natural chlorites may be projected to the compositional space bounded by clinochlore, chamosite, amesite and Mg sudoite [$(Si_3Al)(Al_3Mg_2)O_{10}(OH)_8$]. However, the Margules parameters for interaction on all sites except for M1 were fixed a priori and thus restricted the mixing of the phase components to the M1 site. In a subsequent development, Lanari et al. (2014) retrieved empirical symmetric interaction parameters, based on published chlorite analyses, for the 3-site mixing model. Some of these chlorite solid solution models (e.g., Holland et al., 1998; Vidal et al. 2001, 2005;

Lanari et al. 2014) have, however, been developed for conditions corresponding to greenschist facies or higher metamorphic conditions.

In the ideal site-mixing solid solution models (Helgeson and Aagaard, 1985), the cations are presumed to mix on energetically-equivalent sites with consequent resolution of structural sites in the chlorite solid solution into tetrahedral and octahedral sites; the activity (a_i) of the i^{th} thermodynamic component of the solid solution is given by

$$a_i = k_j \prod_s \prod_j \left(X_{j,s}\right)^{\nu_{s,j,i}}$$

where k_i is a proportionality constant, $X_{j,s}$ is the mole fraction of the j^{th} atom on the s^{th} crystallographic site in the solid solution, and $\nu_{s,j,i}$ is the stoichiometric number of the s^{th} sites occupied by the j^{th} atom in one mole of the i^{th} thermodynamic component. The ideal site-mixing model has been applied rather extensively (Walshe, 1986; Jahren and Aagaard, 1992; Saccocia and Seyfried, 1994; Aja, 2002). Walshe (1986) implemented an ideal site-mixing model for chlorites from hydrothermal alteration environments using a set of six end-member components [$Mg_6Si_4O_{10}(OH)_8$, $Mg_5Al_2Si_3O_{10}(OH)_8$, $Fe_5^{2+}Al_2Si_3O_{10}(OH)_8$, $Fe_5^{2+}Fe_2^{3+}Si_3O_{10}(OH)_8$, $Al_4Si_4O_{10}(OH)_8$, and $Fe_4^{2+}Fe^{3+}Al_2Si_3O_{11}(OH)_7$]. Saccocia and Seyfried (1994) modeled their higher temperature (300° - 500° C) chlorite solubility data with an ideal site-mixing of a clinochlore-chamosite solid solution. Similarly, the solubility data from the lower temperature hydrothermal experiments of Aja and co-workers have also been modeled using the ideal site mixing model for a chamosite – clinochlore solid solution; values of $\log\frac{a_{Mg^{2+}}^{1/2}}{a_{H^+}}$ calculated for the experimental chlorite + kaolinite + quartz + fluid assemblages differed significantly at 25 °C from measured values (cf. Figure 2; Aja, 2002) but converged towards the measured values with increasing temperatures ($T \geq 200$ °C).

These chlorite solid solution models generally adopt *putative* structural chemistries based on general chlorite stoichiometry rather than on *exact* atomic site occupancies of the particular samples being investigated. The use of putative chemistry reflects the lack of detailed specific knowledge of the exact structural chemistry of each chlorite sample being studied and is in turn a reflection of the types of chemical and mineralogical data available during petrogenetic and/or lithochemical studies and the prohibitive work of determining atomic site occupancies for each chlorite sample being studied. Nonetheless, configurational entropy of chlorites is solely a function of the actual atomic site occupancies and makes a significant contribution to third law entropy (Aja et al., 2015).

Past models of chlorite solid solution have thus presumed to effect cation mixing on crystallographically distinct sites; these models have been implemented by either the mixing of cations on a single site or some adaptation of multisite mixing models. However, cation distributions in the chlorites are usually not known a priori and hence the need for putative atomic site assignments. A molecular solid solution model, by contrast, offers an alternative approach. In this approach, presumptions of putative atomic site occupancies of the chlorites under investigation are circumvented; rather, a single aggregate parameter serves as an index to the contribution of a particular endmember phase to the solid solution. The adoption of molecular (or endmember) mole fractions presumes that local charge balance is maintained in the structure of the mineral which in this case is consistent with the short-range order shown by cation occupancies in the chlorite structure.

The particular molecular approach being proposed is chemographically derived based on the compositional signatures of natural chlorites captured in the classic work of Foster (1962). Plotting the variation of tetrahedral Al as a function of $\frac{Fe^{2+}}{R^{2+}}$ ratio (Figure 3a), the Fe-Mg chlorites may be separated into Al-rich and Si-rich varieties along the continous clinochlore-chamosite binary join; the chlorites having $Al^{IV} > 1/O_{10}(OH)_8$ are denoted as Al-rich whereas Si-rich chlorites are those having $Al^{IV} < 1/O_{10}(OH)_8$ (Aja, 2015). The varying deviation of tetrahedral Al from the chamosite-clinochlore binary is employed as an index to solid substitutions away from the binary join; this deviation is then set equal to the mole composition of either amesite or Al-free chlorite in the solid solution and thus implicitly incoporates the Tschermak substitution vectors of natural chlorites. Given that the mole fraction of amesite or Al-free chlorite quantifies the Tschermak substitution away from the chamosite – clinochlore binary join, these ternary models embody both the Fe-Mg_{-1} exchange vector and the Tschermak substitution vectors of natural chlorites.

In this molecular approach, solid solutions of Al-rich Fe-Mg chlorites are modeled in terms of the endmembers amesite [$(Mg_4Al_2)(Si_2Al_2)O_{10}(OH)_8$], chamosite [$(Fe_5Al)(Si_3Al)O_{10}(OH)_8$] and clinochlore [$(Mg_5Al)(Si_3Al)O_{10}(OH)_8$]. For such chlorites, mole components in the ternary solid solutions are determined as follows:

$X_{amesite} = [Al^{IV}/O_{10}(OH)_8 - 1]$,

$X_{chamosite} = (X_{Fe})(1-X_{amesite})$ and

$X_{clinochlore} = 1 – (X_{amesite} + X_{chamosite})$

By contrast to the Al-rich chlorites, chlorite solid solutions for Si-rich Fe-Mg chlorites $[Al^{IV} < 1/O_{10}(OH)_8]$ may be modeled in terms of the end-members Al-free chlorite $[Mg_6Si_4O_{10}(OH)_8]$, chamosite $[(Fe_5Al)(Si_3Al)O_{10}(OH)_8]$ and clinochlore $[(Mg_5Al)(Si_3Al)O_{10}(OH)_8]$. In this case, the mole components in the ternary solid solutions are computed as follows:

$X_{Al\text{-}free\ chlorite} = [1 - Al^{IV}/O_{10}(OH)_8]$,

$X_{chamosite} = (X_{Fe})(1-X_{Al\text{-}free\ chlorite})$ and

$X_{clinochlore} = 1 – (X_{Al\text{-}free\ chlorite} + X_{chamosite})$

Using the above parameters, the chlorite compositional data from figure 3a have been projected onto the the amesite-chamosite-clinochlore system (Figure 3b) and Al-free chlorite-chamosite-clinochlore system (Figure 3c); also depicted in figures 3b and 3c are the compositions of calorimetrically-investigated natural chlorites (see Table 2) projected onto the ternary compositional space. Evidently, these ternary systems provide a compositional space within which to portray natural chlorite compositions.

The ternary solid solution, however, does not account for the substitutional effects of octahedral vacancies and hence di-trioctahedral chlorite substitutions; this is achieved in this molecular approach by projecting chlorite compositions into the quaternary amesite $[(Mg_4Al_2)(Si_2Al_2)O_{10}(OH)_8]$, chamosite $[(Fe_5Al)(Si_3Al)O_{10}(OH)_8]$, clinochlore $[(Mg_5Al)(Si_3Al)O_{10}(OH)_8]$ and sudoite $(Mg_2Al_3\square_1)(Si_3Al)O_{10}(OH)_8$ system for Al-rich chlorites and the quaternary Al-free chlorite [$Mg_6Si_4O_{10}(OH)_8$], chamosite [$(Fe_5Al)(Si_3Al)O_{10}(OH)_8$], clinochlore [$(Mg_5Al)(Si_3Al)O_{10}(OH)_8$] and sudoite $(Mg_2Al_3\square_1)(Si_3Al)O_{10}(OH)_8$ system for Si-rich chlorites. In the quaternary amesite-chamosite-clinochlore-sudoite solid solution, mole components are then defined as (Aja, 2016):

$X_{amesite} = [Al^{IV}/O_{10}(OH)_8 - 1]$,

$X_{chamosite} = (X_{Fe})(1-X_{amesite})$,

$X_{sudoite} = X_{\square}$ (mole fraction of octahedral vacancy) and

$X_{clinochlore} = 1 - (X_{amesite} + X_{chamosite} + X_{sudoite})$

An analogous formalism applies to Si-rich chlorites in the quaternary system consisting of the endmembers Al—free chlorite, chamosite, sudoite and clinochlore; in this quaternary system, $X_{amesite}$ is replaced by $X_{Al\text{-}free\ chlorite}$.

One of the advantages of modeling natural chlorites using two complementary solid solutions is that it implicitly recognizes the importance of bulk rock compositions in chlorite mineralizations; this may facilitate the development of less complex thermodynamic models of chlorite geothermometry especially under diagenetic/low temperature hydrothermal conditions given that lithological effects is likely to be more significant at lower temperatures (T < 300 °C). Indeed, owing to the ubiquity of chlorites in a wide variety of diagenetic and/or low temperature geological settings, the geothermometric potential of chlorites has been of perennial interest (e.g., Cathelineau and Nieva, 1985; Kranidiotis and McLean, 1987; Cathelineau, 1988; Hillier and Velde, 1991; De Caritat, 1993; Vidal et al, 2001; Inoue et al. 2009; Bourdelle et al. 2013a, b;

Lanari et al., 2014). The earliest efforts in the development of chlorite geothermometers sought to use a compositional parameter (e.g., tetrahedral Al content) as a geothermometer though such approaches failed to account for lithological effects on chlorite compositional variations. Latter efforts have sought to develop chlorite geothermometers using thermodynamic models of chlorite solid solutions though for such treatments, reliable activity composition models calibrated with experimental thermochemical data does not yet exist.

Excess Thermodynamic Properties

The excess entropy of mixing amesite, chamosite and clinochlore to yield compositions equivalent to the natural chlorites whose calorimetric entropies are known (Table 2), calculated using equation 6, decreases curvilinearly with increasing $X_{clinochlore}$ (Fig. 4a) whereas it appears to increase somewhat curvilinearly with increasing mole fraction of chamosite up to $X_{chamosite} \cong 0.6$ (Fig. 4b). S^{ex} appears to also increase with increasing mole fraction of amesite (Fig. 4c) though the trend is masked by the clustering around $X_{amesite} \approx 0.3 - 0.4$; this clustering reflects the accidental bias in the amesite component of the chlorite samples that have been investigated calorimetrically (diamonds; Fig. 3a and 3b). Within this narrow amesite content, there is a spread of about 60 J/mol•K suggesting that the solid solution interaction parameters for these individual chlorite samples may not be same. As to be expected, significantly different entropies of mixing result if S_{298} of endmember phases obtained from different datasets are used (Aja, 2015); nonetheless, the pattern of dependencies on mole fraction components is the same regardless of the data source (e.g., Holland and Powell, 1998 vs. Vidal et al. 2005). On the whole, the curvilinear trends apparent in Fig. 4 may indicate some volume correlation since excess vibrational entropies of solid solutions are known to show a correlation with molar volume and bulk modulus of limiting endmember phases (cf. Benisek and Dachs, 2012) and the correlation of entropy with volume is a well-established concept (Holland, 1989).

A comparison of the excess entropies of mixing calculated for the ternary amesite-chamosite-clinochlore systems and for the quaternary amesite-chamosite-sudoite-clinochlore system (Fig. 5a) shows these to be virtually of the same magnitudes suggesting that the di-trioctahedral substitution has a marginal effect on S^{ex}. In other words, the energetics of chlorite solid solutions is dominated by Fe-Mg exchange and Tschermak substitutions.

By contrast to calorimetric entropy, standard state Gibbs free energies of formation are less readily available for chlorites; hence, equation 7 could only be applied to determine the excess Gibbs energy of mixing for stoichiometric equivalents of CCa-2, Fe-Chl(W), Mg-Chl and two other samples from Kittrick (1982). The calculated G_{ss}^{ex} vary from about -72 to 413 kJ/mol (Fig. 5b) implying a significant deviation from ideality. However, the linear dependence for G_{ss}^{ex} on $X_{clinochlore}$ (Fig. 5b) may be more apparent than real considering that these points are not, in fact, co-planar in the G^{ex} - X_{Clc} plane inasmuch as they have different mole fractions of other component endmembers. Nonetheless, the minor effect of the di-trioctahedral substitution on the energetics of chlorite solid solutions is underscored by the magnitudes of excess Gibbs energy calculated in both the ternary and quaternary systems.

Conceivably, the ternary clinochlore (Clc) - chamosite (Chm) - amesite (Ame) solid solution could be modeled either as a symmetric or asymmetric ternary solid solution; in the former case, the Margules parameters may be retrieved using Eqn. 8; that is,

$$\mathrm{G_{ss}^{ex}} = \mathrm{W_{G_{Clc-Chm}} X_{Clc} X_{Chm}} + \mathrm{W_{G_{Chm-Ame}} X_{Chm} X_{Ame}} + \mathrm{W_{G_{Clc-Ame}} X_{Clc} X_{Ame}} \quad (8)$$

For an asymmetric ternary solid solution, Eqn. 9 applies.

$$\begin{aligned}\mathrm{G_{ss}^{ex}} = {} & \left(\mathrm{W_{G_{Clc-Chm}} X_{Clc}^2 X_{Chm}} + \mathrm{W_{G_{Chm-Clc}} X_{Chm}^2 X_{Clc}}\right) + \\ & \left(\mathrm{W_{G_{Chm-Ame}} X_{Chm}^2 X_{Ame}} + \mathrm{W_{G_{Ame-Chm}} X_{Ame}^2 X_{Chm}}\right) + \\ & \left(\mathrm{W_{G_{Clc-Ame}} X_{Clc}^2 X_{Ame}} + \mathrm{W_{G_{Ame-Clc}} X_{Ame}^2 X_{Clc}}\right) \qquad (9)\end{aligned}$$

However, with only five G_{ss}^{ex} data points (Fig. 5b), analytical determination of the ternary solid solution interaction parameters from the functional dependence of $\mathrm{G^{ex}}$ on mole compositions (Eqns 8 or 9) will not be meaningful owing to the considerable likelihood of over-fitting the data. The sparsity of G_{ss}^{ex} reflects the very limited number of studies from which a full complement of thermodynamic properties have been retrieved for natural chlorites. Furthermore, the range of the Tschermak component of natural chlorites that have been studied by calorimetry is rather limited compared to the Fe-Mg compositional range (cf. Fig. 3a); perhaps, this reflects the bias in favor of Fe-Mg variation in designing thermochemical experiments. Chlorite compositions that deviate from the chamosite-clinochlore join [i.e., $\mathrm{Al^{IV}} = 1/\mathrm{O_{10}(OH)_8}$; Fig. 3] may, however, not be presumed a priori to have same solid solution energetics owing to the different magnitudes of their Tschermak substitution vectors and thus thermochemical studies designed principally to span the characteristic wide Fe-Mg range may not have afforded adequate access to the complete spectrum of chlorite solid solution behavior.

It becomes apparent that for this major group of minerals (i.e., chlorites), a significant gap exists in the body of experimentally-derived thermochemical data. Calorimetric studies of chlorites are much more abundant than studies in which a full complement of chlorite thermodynamic properties have been determined, and even in that instance, the natural chlorites that have been studied calorimetrically do not cover the spectrum of known compositions. Perhaps, this limitation has not been readily apparent given the advent of correlation algorithms and the increasing sophistication of computational technologies. In fact, Oelkers et al. (2009) highlighted the relative sparsity of actual experimental data on which some thermodynamic datasets are based owing to the increasing use of computerized correlation algorithms; in other words, the success and widespread use of aqueous chemical speciation, reaction path and transport computer codes have obscured the provisional nature of some of the thermodynamic databases built into these algorithms.

Neoformation of Fe-chlorite

Diagenetic chlorites may form as rims on framework grains leading to the preservation of abnormally high porosity in petroleum reservoir sandstones; chlorites may also form as grain-coating or pore-filling materials in such reservoirs. In sandstones, chlorite authigenesis has been attributed to transformation of 7 Å, ferroan, green clays to chamosite, concomitant dissolution of kaolinite and ferroan carbonates or organometallic iron compounds (Bloch et al. 2002; Gould et al. 2010). In addition, chlorite neoformation via alteration of precursor minerals have also been proposed and includes alteration of berthierine, mixed-layer serpentine-chlorite, kaolinite, smectite, iron- and magnesium-rich detrital grains and volcanic rock fragments and from mud intraclasts (Dowey, 2012 and references therein; Beaufort et al. 2015).

Both iron-rich and magnesium-rich chlorites have been reported in siliciclastic lithologies; however, the former occurs much more frequently (Bloch et al. 2002; Dowey, 2012). The occurrences of Fe-rich chlorite coats have been attributed to provenance-control resulting from in situ alteration of volcanic (lithic) rock fragments. Fe-rich chlorites are also thought to occur dominantly in coastal environments whereas magnesium-rich chlorites have been linked to desert aeolian or playa lake environments (Dowey, 2012). Ehrenberg (1993) suggested that influent amorphous iron hydroxides, brought in by riverine transport, flocculated upon mixing with seawater and thus facilitates the formation of iron-rich chlorites in sandstones inasmuch as chlorite-coated sandstones are typical of nearshore marine facies likely to have been influenced by riverine water influx.

A precursor material that hitherto has not been considered in the various models for the neoformation of Fe-rich chlorites in sandstones is inherited green rusts. Perhaps, the reason that the preponderance of authigenic chlorites tend to be Fe-rich is the influence of green rusts. Green rusts typically occur as iron corrosion products and includes carbonate green rust 1, $GR1(CO_3^{2-})$ or $[Fe_4^{2+}Fe_2^{3+}(OH)_{12}][CO_3 \bullet 2H_2O]$. The general formula for carbonate green rust is$[Fe_x^{2+}Fe_2^{3+}(OH)_{2x+4}][CO_3 \bullet (x-2)H_2O$; the value of x lies between 4-6 (Drissi et al. 1995). Structurally, $GR1(CO_3^{2-})$ is a member of the pyroaurite group of hydroxides though the latter is a Mg^{2+}/Fe^{3+} hydroxy carbonate. Green rusts have also been shown to occur in soils (Feder et al., 2005; Trolard et al., 2007) and may exercise significant influence in formation of iron oxides in the soils. In other studies, green rusts have been shown to form near the iron redoxcline and may persist in aquatic environments through the water column and in ferruginous sediments; moreover, they transform into several of the major minerals observed in iron formations (Halevy et al. 2017). It is thus quite likely that an important part of the global iron cycle would include the transformation of green rusts into berthierines and chlorites under diagenetic conditions.

Using Eh-pH diagrams (Fig. 6), stability relationships between Fe-rich chlorite minerals and green rusts have been evaluated at 25 °C. In this model (Fig. 6), aqueous ion activities of $Al^{3+}_{(aq)}$, $Fe^{2+}_{(aq)}$, $Mg^{2+}_{(aq)}$, $SiO_{2(aq)}$ and $CO^{2-}_{3(aq)}$ were held at $7.9\text{x}10^{-6}$, $5.01\text{x}10^{-6}$, $4.57\text{x}10^{-3}$, $1.95\text{x}10^{-3}$ and $1.95\text{x}10^{-2}$, respectively; the thermodynamic properties of the species used in calculating Fig. 6 are given in Table 3. The aqueous ion activities were representative of conditions in which chlorites equilibrated in some of our earlier experiments at 25 °C. Under the conditions of this analysis, $GR1(CO_3)^{2-}$ is shown to have a wider stability field relative to pyroaurite. It is also apparent from figure 3c that the two Fe-rich chlorites with contrasting mole fractions of Fe [Fe-Chl(W)_{adj} and CCa-2*] will be stable under rather different redox-pH conditions; at the same Eh, increasing acidity favors the neoformation of the chlorite having a higher Fe content. Perhaps, the greater incidence of authigenic Fe chlorites, relative to Mg chlorites, may also reflect the influence of somewhat acidic pore waters. As to be expected, green rusts would readily transform to berthierine and Fe-chlorites although $GR1(CO_3)^{2-}$ has a slightly wider field of stability in the presence of berthierine (Fig. 6b) relative to Fe chlorite (Fig. 6c) suggesting that it may transform to the former less readily. Nonetheless, at appropriate aqueous solute activities and redox conditions, green rusts will readily transform to berthierines or Fe-chlorites in aqueous media.

Green rusts in sediments may thus serve as important precursors of some pore-filling or grain coatings chlorites in siliciclastic sediments. Such green rust precursors may be delivered as inherited clastic sediments infiltrating sandstones inasmuch as infiltration of sandstones by allogenic materials is an established sedimentary process (Ali et al. 2010). The multivalent state of Fe in green rusts would provide an explanation for the multivalent state of Fe in most sedimentary chlorites. However, the lability of green rusts may have hitherto hindered its detection in such sedimentary sequences. On the whole, whether green rusts are precursors of minerals found in iron formations (Zegeye et al. 2012; Halevy et al. 2017) or are precursors of sedimentary chlorites (this study) will reflect controls exercised by factors such as pH, aqueous chemistry of the pore fluids, redox conditions, pressure, and temperature.

Implications

The use of chlorite composition as a geothermometer has been a subject of perennial interest especially in diagenetic and low temperature hydrothermal environments. However, such geothermometric applications of chlorite compositions has met with limited success and has also been questioned owing to the lack of reliable activity composition models calibrated with experimental thermodynamic data. The molecular approach proposed herein may provide the context for the thermodynamic calibration of chlorite geothermometers and also constitutes an alternative viable approach to atomic site-mixing models inasmuch as knowledge of exact atomic site occupancies of the chlorites, which is typically unavailable, is not required. Though further development of chlorite geothermometers rooted in experimentally-derived activity composition models is currently hampered by the sparsity of measured excess Gibbs energy of mixing, the ternary solid solution model nonetheless provides a compact chemography for petrographic and lithogeochemical descriptions. For instance, the amesite-clinochlore-chamosite compositional space fully define the limits of chlorite alteration from the Phelps Dodge massive sulfide deposit in Québec (cf. Fig. 9; Kranidiotis and MacLean, 1987).

.

Calorimetric entropies (S_{298}) are routinely extracted from calorimetric measurements though third law entropies (S°_{298}) are, in fact, more apposite for petrogenetic models. Amongst all the natural chlorites that have been investigated heretofore by calorimetry, third law entropy has been determined only for two samples [Fe-Chl(W) and Mg-Chl; Aja et al. 2015] and these show that configurational entropy owing to atomic site occupancies is a significant component of third law entropy. Given the virtual nonexistence of experimental third law entropies, enthalpy of formation and third law entropy of chlorite endmembers have had to be treated as adjustable properties in some petrogenetic models. This may be a practical necessity that reflects current state of knowledge of standard state properties; nonetheless, *ad hoc* adjustments of fundamental thermodynamic properties in order to assure meaningful petrogenetic conclusions leave much to be desired. The scientific quest for an evolving knowledge of standard states properties of the chlorite group of minerals mandates highlighting this deficiency and the need for more exhaustive affirmative experimental determinations of standard state thermochemical properties ($\Delta_f G^{\circ}_{298,1}$, $\Delta_a G^{\circ}_{T,i}$, $S^{\circ}_{298,1}$ and C°_p) of minerals of the chlorite group.

Acknowledgements

Part of this study was supported by a grant from the Petroleum Research Fund administered by the American Chemical Society (ACS-PRF# 29930-AC2) and by the University Committee on Research Awards (PSC – CUNY: RF No. 6-66205, 6-667208) Program. Travel grants provided by the Office of the Dean, School of Natural and Behavioral Sciences (Brooklyn College) are also acknowledged. Thoughtful and constructive review comments provided by Dr. Benoit Dubacq and other journal reviewers are gratefully acknowledged.

References

Aja, S. U. (2002) The stability of Fe-Mg chlorites in hydrothermal solutions: II. Thermodynamic properties. Clays and Clay Minerals, 50, 591-600.

Aja, S. (2015) A ternary solid solution model of natural chlorites. Geological Society of America Abstracts with Programs. Vol. 47, No. 7, p.819.

Aja, S. (2016) Chlorite thermochemistry: insights from combining calorimetric and solution equilibration data. Programs & Abstracts, 53rd Annual Meeting of the Clay Minerals Society, p. 1

Aja, S.U. and Dyar M. D. (2002) The stability of Fe-Mg chlorites in hydrothermal solutions – I. Results of experimental investigations. Applied Geochemistry,17, 1219-1239.

Aja, S.U. and Small, J.S. (1999) The solubility of a low-Fe clinochlore between 25 and 175 °C and $P_v = P_{H2O}$. European Journal of Mineralogy, **11**, 829-842

Aja, S., Omotoso, O., Bertoldi, C., Dachs, E., and Benisek, A. (2015) The structure and thermochemistry of three Fe-Mg chlorites. Clays and Clay Minerals, 63, 351 – 367.

Ali, A.A., Clark, W.J. and Dribus, J. R. (2010) Diagenesis and reservoir quality. Oilfield Reviews, 22, 14-27.

Anderson, G. M. and Crerar, D. A. (1993) Thermodynamics in Geochemistry: The Equilibrium Model, 588 pp. Oxford University Press, New York.

Bahlis, A.B. and De Ros, L.F. (2013) Origin and impact of authigenic chlorite in the Upper Cretaceous sandstone reservoirs of the Santos Basin, eastern Brazil. Petroleum Geoscience, 19, 185-189.

Bailey, S. W. (1988) Chlorites: Structure and crystal chemistry. Reviews in Mineralogy 19, 347-403.

Bartier, D., Bautier, M., Lopez, M., Potdevin, J. L., Chamley, H. and Arostegui, J. (1998) Lithological control on the occurrence of chlorite in the diagenetic Wealden complex of the Bilbao anticlinorium (Basco-Cantabrian basin, Northern Spain). Clay Minerals, 33, 317-332.

Beaufort, D., Rigault, C., Billon, S., Billault, V., Inoue, A., Inoue, S. and Patrier, P. (2015) Chlorite and chloritization processes through mixed-layer mineral series in low-temperature geological systems – a review. Clay Minerals 50, 497-523.

Benisek, A. and Dachs, E. (2012) A relationship to estimate the excess entropy of mixing: Application in silicate solid solutions and binary alloys. Journal of Alloys and Compounds, 527, 127 – 131.

Berger, A., Gier, S. and Krois, P. (2009) Porosity-preserving chlorite cements in shallow-marine volcaniclastic sandstones: Evidence from Cretaceous sandstones of the Sawan gas field, Pakistan. American Association of Petroleum Geology Bulletin, 93, 595-615.

Bertoldi, C., Benisek, A., Čemic, L. and Dachs, E. (2001) The heat capacity of two natural chlorite group minerals derived from differential scanning calorimetry. Physics and Chemistry of Minerals, 28, 332-336.

Bertoldi, C., Dachs, E. and Appel, P. (2007) Heat pulse calorimetry on natural chlorite-group minerals. American Mineralogist, 92, 553-559.

Blanc, P. Gailhanou, H., Rogez, J., Mikaelin, G., Kawaji, H., Warmont, F., Gaboreau, S., Grangeon, S., Grenèche, J-M., Vieillard, P., Fialips, C. I., Giffaut, E., Gaucher, E.C. and Claret, F. (2014) Thermodynamic properties of chlorite and berthierine derived from calorimetric measurements. Physics and Chemistry of Minerals, 41, 603-615.

Bloch, S., Lander, R.H. and Bonnell, L. (2002) Anomalously high porosity and permeability in deeply buried sandstone reservoirs: Origin and predictability. American Association of Petroleum Geology Bulletin, 86, 301-328.

Bourdelle, F., Parra, T., Chopin, C. and Beyssac, O. (2013a) A new chlorite geothermometer for diagenetic to low-grade metamorphic conditions. Contributions to Mineralogy and Petrology, 165, 723 -725.

Bourdelle, F., Parra, T., Chopin, C., Beyssac, O. and Vidal, O. (2013b) Clay minerals as geo-thermometer: A comparative study based on high spatial resolution analyses of illite and chlorite in Gulf Coast sandstones (Texas, U.S.A.). American Mineralogist, 98, 914-926.

Cathelineau, M. (1988) Cation site occupancy in chlorites and illites as a function of temperature. Clay Minerals, 23, 471–485

Cathelineau, M. and Nieva, D. (1985) A chlorite solid solution geothermometer. The Los Azufres (Mexico) geothermal system. Contributions to Mineralogy and Petrology, 91, 235–244.

De Caritat, P., Hutcheon, I., and Walshe, J.L. (1993) Chlorite geothermometry: a review. Clays and Clay Minerals, 41, 219–239.

Dowey, P. J. (2012) Prediction of clay minerals and grain-coatings in sandstone reservoirs utilizing ancient examples and modern analogues, 377 pp. *Ph.D. Thesis*, University of Liverpool.

Drissi, S. H., Refait, Ph., Abdelmoula, M. and Génin, J. M. R. (1995) The preparation and thermodynamic properties of Fe(II)-Fe(III) hydroxide-carbonate (green rust 1); Pourbaix diagram of iron in carbonate-containing aqueous media. Corrosion Science 37, 2015 - 2041.

Ehrenberg, S.N. (1993) Preservation of anomalously high porosity in deeply buried sandstones by grain-coating chlorite; Examples from Norwegian Continental Shelf: American Association of Petroleum Geology Bulletin, 77, 1260–1286.

Feder, F., Trolard, F., Klingelhö, G. and Bourrié, G. (2005) In situ Mössbauer spectroscopy: Evidence for green rust (fougerite) in a gleysol and its mineralogical transformations with time and depth. Geochimica et Cosmochimica Acta, 69, 4463–4483

Foster, M. D. (1962) Interpretation of the composition and classification of chlorites. Geological Survey Professional Paper, 414-A, 1-33.

Gailhanou, H., Rogez, J., van Miltenburg, J.C., van Genderen, A.C.G., Greńche, J.M., Gilles, C., Jalabert, D., Michau, N., Gaucher, E.C. and Blanc, P. (2009) Thermodynamic properties of chlorite CCa-2. Heat capacities, heat contents and entropies. Geochimica et Cosmochimica Acta **7**3, 4738 – 4749.

Gailhanou, H., Blanc, P., Rogez, J., Mikaelian, G., Horiuchi, K., Yamamura, Y., Saito, K., Kawaji, H., Warmont, F., Greńche, J.M., Vieillard, F., Fialips, CI., Giffaut, E. and Gaucher, E.C. (2013) Thermodynamic properties of saponite, nontronite, and vermiculite derived from calorimetric measurements. American Mineralogist, 98, 1834-1847.

Gould, K., Pe-Piper, G. and Piper, D.J.W. (2010) Relationship of diagenetic chlorite rims to depositional facies in Lower Cretaceous reservoir sandstones of the Scotian basin. Sedimentology, 57, 587-610.

Grisby, J.D. (2001) Origin and growth mechanism of authigenic chlorite in sandstones of the Lower Vicksburg Formation, South Texas. Journal of Sedimentary Research, 71, 27-36.

Halevy, I., Alesker, M., Schuster, E. M., Popovitz-Biro, R and Feldman, I. (2017) A key role for green rust in the Precambrian oceans and the genesis of iron formations. Nature Geoscience, http://dx.doi.org/10.1038/ngeo2878

Helgeson, H.C. and Aagaard, P. (1985) Activity/composition relations in among silicates and aqueous solutions: I. Thermodynamics of intrasite mixing and substitutional order/disorder in minerals. American Journal of Science 285, 769-844.

Hemingway, B.S., Kittrick, J.A., Grew, E.S., Nelen, J.A. and London, D. (1984) The heat capacity of osumilite from 298.15 to 1000 K, the thermodynamic properties of natural chlorites to 500 K, and the thermodynamic properties of petalite to 1800 K. American Mineralogist 69, 701-710.

Hillier, S. (1994) Pore-lining chlorites in siliciclastic reservoir sandstone: electron microprobe, SEM and XRD data, and implications for their origin. *Clay Minerals*, 29, 665-679.

Hillier, S. and Velde, B. (1991) Octahedral occupancy and the chemical-composition of diagenetic (low-temperature) chlorites. Clay Minerals, 26, 149–168.

Holland, T. J. B. (1989) Dependence of entropy on volume for silicates and oxide minerals: A review and a predictive model. American Mineralogist, 74, 5 – 13.

Holland, T.J.B. and Powell, R. (1998) An internally consistent thermodynamic dataset for phases of petrological interest. Journal of Metamorphic Geology 16, 309-343.

Holland, T., Baker, J. and Powell, R. (1998) Mixing properties and activity-composition relationships of chlorites in the system $MgO-FeO-Al_2O_3-SiO_2-H_2O$. European Journal Mineralogy, 10, 395-406.

Holland, T.J.B. and Powell, R. (2011) An improved and extended internally consistent thermodynamic dataset for phases of petrological interest, involving a new equation of state for solids. Journal of Metamorphic Geology, 29, 333–383

Inoue, A., Meunier, A., Patrier-Mas, P., Rigault, C., Beaufort, D., and Vieillard, P. (2009) Application of Chemical geothermometry to low-temperature trioctahedral chlorites. Clays and Clay Minerals, 57, 371–382.

Jahren, J.S. and Aagaard, P. (1992) Diagenetic illite-chlorite assemblages in arenites. II. Thermodynamic relations. Clays and Clay Minerals, 40, 547-554.

Kampman, N., Bickle, M., Wigley, M. and Dubacq, B. (2014) Fluid flow and CO_2-fluid mineral interactions during CO_2-storage in sedimentary basins. Chemical Geology, 369, 22 – 50.

Kittrick, J.A. (1982) Solubility of two high-Mg and two high-Fe chlorites using multiple equilibria. Clays and Clay Minerals, 30, 167-179.

Kranidiotis, P. and McLean, W.H. (1987) Systematics of chlorite alternation at the Phelps Dodge massive sulfide deposit, Matagami, Quebec. Economic Geology, 82, 1898–1911.

Lammers, L.N., Brown Jr., G.E., Bird, D.K., Thomas, R.B., Johnson, N.C., Rosenbauer, R. J., and Maher, K. (2015) Sedimentary reservoir oxidation during geologic CO_2 sequestration. Geochimica et Cosmochimica Acta, 155, 30–46.

Lanari, P., Wagner, T. and Vidal, O. (2014) A thermodynamic model for di-trioctahedral chlorite from experimental and natural data in the system $MgO-FeO-Al_2O_3-SiO_2-H_2O$: applications to P-T sections and geothermometry. Contributions to Mineralogy and Petrology, 167: 968-

Lu J., Kharaka, Y.K., Thordsen, J.J., Horita, J., Karamalidis, A., Griffith, C., Hakala, A. Ambats, G., Cole D.R., Phelps, T.J., Manning, M.A.., Cook, P.J. and Hovorka, S.D. (2012) CO_2–rock–brine interactions in Lower Tuscaloosa Formation at Cranfield CO_2 sequestration site, Mississippi, U.S.A. Chemical Geology, 291 269–277

Oelkers, E. H., Helgeson, H. C., Shock, E. L., Sverjensky, D. A. and Pokrovskii, V. A. (1995) Summary of the apparent standard partial molal Gibbs free energies of formation of aqueous species, minerals, and gases at pressures 1 to 500 bars and temperatures 25 to 1000 °C. Journal of Physics and Chemical Reference Data, 24, 1401- 1560

Oelkers, E. H., Bénézeth, P. and Pokrovski, G. S. (2009) Thermodynamic databases for water-rock interaction. Reviews in Mineralogy and Geochemistry, 70, 1-46.

Ogorodova, L. P., Vigasina, M. F., Melchakova, L. V., Kiseleva, I., Krupskaya, V. V. and Bryzgalov, I. A. (2016) Natural Fe-Mg clinochlores: enthalpies of formation and dehydroxylation derived from calorimetric study. American Mineralogist, 101, 1431-1437.

Robie, R. A. and Hemingway, B.S. (1995) Thermodynamic Properties of Minerals and Related Substances at 298.15 K and 1 Bar (105 Pascals) Pressure and at Higher Temperatures. U.S. Geological Survey Bulletin 2131, 461 pp.

Rozov, K., Berner, U., Kulik, D. and Diamond, L.W. (2009) Solubility and thermodynamic properties of carbonate-bearing hydrotalcite-pyroaurite solid solutions with a 3:1 Mg/(Al+Fe) ratio. Clays and Clay Minerals, 59, 215–232.

Saccocia, P. J. and Seyfried, Jr. W.E. (1994) The solubility of chlorite solid solutions in 3.2 wt% NaCl fluids from 300 – 400 °C, 500 bars. Geochimica et Cosmochimica Acta, 58, 567 – 585.

Stoessell, R. K. (1984) Regular solution site-mixing model for chlorites. Clays and Clay Minerals, 32, 205 - 212.

Smyth, J. R., Darby Dyar, M., May, H. M., Bricker, O. P. and Acker, J. (1997) Crystal structure and Mossbauer spectroscopy of an ordered, triclinic clinochlore. Clays and Clay Minerals, 45, 544 – 550.

Tetiker, S., Yalçın, H., Bozkaya, Ö. (2015) Approaches to Low Grade Metamorphic Evolution of Karakaya Complex with Chlorite Mineralogy and Geochemistry. Minerals, 5, 221-246.

Trolard, F., Bourrié, G., Abdelmoula, M., Refait, P. and Feder, F. (2007) Fougerite, a new mineral of the pyroaurite-iowaite group: description and crystal structure. Clays and Clay Minerals, 3, 323 - 334.

Ulbrich, H.H. and Waldbaum, D.R. (1976) Structural and other contributions to the third-law entropies of silicates. Geochimica et Cosmochimica Acta, 40, 1 - 24.

Vidal, O., Parra, T. and Trottet, F. (2001) A thermodynamic model for Fe-Mg aluminous chlorite using data from phase equilibrium experiments and natural politic assemblages in the 100 – 600 °C, 1-25 kb range. American Journal of Science, 301, 557-592.

Vidal, O., Parr, T. and Vieillard, P. (2005) Thermodynamic properties of the Tschermak solid solution in Fe-chlorite: Application to natural examples and possible role of oxidation. American Mineralogist, 90, 347 – 358.

Walshe, J. L. (1986) A six-component chlorite solid solution model and the conditions of chlorite formation in hydrothermal and geothermal systems. Economic Geology, 81, 681-703.

Welch, M.D., Barras, J. and Klinowski, J. (1995) A multinuclear NMR study of clinochlore. American Mineralogist, 80, 441 – 447.

Zazzi, A., Hirsch, T.K., Leonova, E., Kaikkonen, A., Grins, J., Annersten, H. and Eded, M. (2006) Structural investigation of natural and synthetic chlorite minerals by X-ray diffraction, Mossbauer spectroscopy and solid state nuclear magnetic resonance. Clays and Clay Minerals, 54, 252-265.

Zegeye, A., Bonneville, S., Benning, L.G., Sturm, A., Fowle, D. A., Jones, C., Canfield, D. E., Ruby, C., MacLean, L. C., Nomosatryo, S., Crowe, S. and Poulton, S.W. (2012) Green rust formation controls nutrient availability in a ferruginous water column. Geology, 40, 599-602.

FIGURE CAPTIONS

Figure 1. Variation of measured calorimetric entropies for natural chlorites at 298.15 K as a function of mole fraction of Fe. The sources of the plotted calorimetric entropies for investigated chlorites are given by citations whereas the mixing lines between chamosite and clinochlore are indicated by the straight lines; HP2011, V2005, HP1998 represent the sources Holland and Powell (2011), Vidal et al. (2005) and Holland and Powell (1998), respectively.

Figure 2. Comparative trends of apparent partial standard Gibbs free energies of formation for three natural chlorites; for CCa-2, the thermodynamic data used in calculation were obtained from Blanc et al. (2014). The solid lines and dot—dashed lines depict apparent Gibbs free energy of formation calculated using calorimetric entropy ($S_{298,1}$) and third law entropy ($S^{\circ}_{298,1}$), respectively.

Figure 3. Compositional spectrum of natural chlorite and compositions of chlorites that have been studied calorimetrically. Chlorite compositions from the classic work of Foster (1962) are shown as black stars whereas solid red diamonds (♦) represent natural chlorites studied calorimetrically: (a) analytical compositions showing variation of tetrahedral Al as a function of mole fraction of Fe^{2+}; (b) composition of Al-rich chlorites projected onto the ternary amesite-chamosite-clinochlore compositional space; (c) compositions of Si-rich chlorites projected onto the ternary Al-free chlorite-chamosite-clinochlore compositional space.

Figure 4. Calculated excess entropies (S^{ex}) in the ternary amesite-chamosite-clinochlore solid solution expressed as a function of the mole fraction of a) clinochlore, b) chamosite and c) amesite. Solid squares (■) represent excess entropies calculated using entropies for endmember phases reported by Holland and Powell (1998). At the 2σ level, the propogated uncertainties fall within the range of ±0.07 to 1.27 J/mol•K and the size of the symbols were chosen to encompass it.

Figure 5. Variation of excess function as a function of mole fraction of clinochlore: (a) S^{ex}; (b) ($G^{ex}_{s.s.}$). G°_{real} for the natural chlorites used in the model include $\Delta_f G^{\circ}_{298,1}$ for Fe-Chl (W), Mg-Chl, CCa-2, and two other samples from Kittrick (1982).

Figure 6. Eh-pH stability relationships between Fe chlorite and green rusts at 25 °C. The Gibbs free energies of formation for ISGS berthierine, Fe-Chl(W) and CCa-2 used in calculating these relationships (Table 2) had been modified to eliminate trace components.

Table 1: Calorimetric entropies ($S_{298,1}$) reported for natural chlorite samples

Samples	Chlorite structural formula per half unit cell	$S_{298,1}$ (J/mol•K)
1. Mg-Chl	$\mathbf{(Si_{2.86}Al_{1.14})(Al_{1.32}Cr^{3+}_{0.003}Fe^{3+}_{0.06}Fe^{2+}_{0.49}Mg_{3.97}Ni_{0.009}\square_{0.148})O_{10}(OH)_8}$	437.81±3.00
2. Fe-Chl (W)	$\mathbf{(Si_{2.62}Al_{1.38})(Al_{1.48}Fe^{3+}_{0.33}Fe^{2+}_{2.73}Mg_{1.19}Mn_{0.02}Zn_{0.007}\square_{0.243})O_{10}(OH)_8}$	499.14±3.40
3. Fe-Chl(M)	$\boldsymbol{(Si_{2.63}Al_{1.37})(Al_{0.97}Ti_{0.14}Fe^{2+}_{3.08}Fe^{3+}_{0.28}Mn_{0.025}Mg_{1.025}Ca_{0.155}P_{0.095}V_{0.005}\square_{0.225})O_{10}(OH)_8}$	515.06±3.60
4. CCa-2	$\boldsymbol{(Si_{2.633}Al_{1.367})(Al_{1.116}Fe^{3+}_{0.215}Fe^{2+}_{1.712}Mg_{2.952}Mn_{0.012}Ca_{0.011})O_{10}(OH)_8}$	469.40±2.90
5. CA	$\mathbf{(Si_{2.64}Al_{1.36})(Al_{1.34}Fe^{3+}_{0.40}Fe^{2+}_{3.52}Mg_{0.50}Mn_{0.006}Ti_{0.005}V_{0.019}Cr_{0.002}Ni_{0.003}Zn_{0.005}Li_{0.014}\square_{0.186})O_{10}(OH)_8}$	548.20±3.78
6. CC	$\mathbf{(Si_{2.64}Al_{1.36})(Al_{1.27}Fe^{3+}_{0.45}Fe^{2+}_{2.35}Mg_{1.65}Mn_{0.056}Ti_{0.002}V_{0.002}Cr_{0.002}Ni_{0.003}Co_{0.001}Zn_{0.005}Li_{0.010}\square_{0.199})O_{10}(O}$	494.30±3.40
7. CD	$\mathbf{(Si_{2.67}Al_{1.33})(Al_{1.29}Fe^{3+}_{0.23}Fe^{2+}_{1.90}Mg_{2.38}Mn_{0.069}Ti_{0.003}V_{0.002}Ni_{0.001}Zn_{0.007}Li_{0.028}\square_{0.90})O_{10}(OH)_8}$	475.70±3.28
8. CE	$\mathbf{(Si_{2.90}Al_{1.10})(Al_{1.05}Fe^{3+}_{0.06}Fe^{2+}_{0.49}Mg_{4.35}Mn_{0.004}Ti_{0.006}Cr_{0.015}Ni_{0.016}Zn_{0.001}\square_{0.008})O_{10}(OH)_8}$	441.90±3.04
9. CF	$\mathbf{(Si_{3.08}Al_{0.92})(Al_{0.89}Fe^{3+}_{0.07}Fe^{2+}_{0.19}Mg_{4.84}\square_{0.01})O_{10}(OH)_8}$	422.80±2.91
10. 21-C	$\boldsymbol{(Si_{2.99}Al_{1.01})(Al_{1.39}Fe^{3+}_{0.21}Fe^{2+}_{0.27}Mg_{3.52}\square_{0.61})O_{10}(OH)_8}$	431.70±5.00
11. 21-D	$\boldsymbol{(Si_{2.47}Al_{1.53})(Al_{1.60}Fe^{3+}_{3.29}Mg_{1.05}\square_{0.06})O_{10}(OH)_8}$	495.70±10.00

Sources of analytical and calorimetric data: samples 1 - 3 (Aja et al. 2015), sample 4 (Blanc et al. 2014), samples 5 - 9 (Bertoldi et al. 2007) and samples 10 - 11 (Hemingway et al. 1984).

Table 2. Standard state thermochemical properties of some chlorites

	Fe-Chl(W)	**Mg-Chl**	**CCa-2**
$C_{p,298}$ (J•mol^{-1}•K^{-1})	**539.62±0.40**	**529.71±0.30**	**547.02±0.27**
$S_{298,1}$ (J•mol^{-1}•K^{-1})	**499.14±3.40**	**437.81±3.00**	**469.40±2.90**
$S^{\circ}_{298,1}$ (J•mol^{-1}•K^{-1})	**578.24±3.80**	**503.21±3.60**	**n.a.**
V (J•bar^{-1})	**21.398**	**20.991**	**21.183**
$\Delta_f G^{\circ}_{298,1}$ (kJ•mol^{-1})	**-7278.97±21.50**	**-8161.76±32.50**	**-7590.73±8.59**
Apparent standard Gibbs free energy of formation, $\Delta_a G^{\circ}_{T,i}$ (kJ•mol^{-1})			
Temperature °C			
50	**-7286.83**	**-8177.58**	**-7603.35**
75	**-7296.47**	**-8195.12**	**-7617.61**
100	**-7307.70**	**-8214.23**	**-7633.40**
125	**-7320.34**	**-8234.78**	**-7650.57**
150	**-7334.29**	**-8256.68**	**-7669.02**
175	**-7349.44**	**-8279.83**	**-7688.67**
200	**-7365.72**	**-8304.19**	**-7709.44**
225	**-7383.07**	**-8329.67**	**-7731.24**
250	**-7401.42**	**-8356.23**	**-7754.01**

$S_{298,1}$ and $S^{\circ}_{298,1}$ denote calorimetric entropy and third law entropy, respectively; n.a. indicates data not available.

Table 3: Standard State Gibbs free energies of formation (kJ/mol)

Name of species		$\Delta_f G^\circ_{298,1}$	**Source of data**
Aluminum ion	Al^{3+}	-487.60	Oelkers et al. (1995)
Carbonate ion	$(CO_3)^{2-}$	-527.98	Oelkers et al. (1995)
Ferrous ion	Fe^{2+}	-91.50	Oelkers et al. (1995)
Water	H_2O	-237.19	Oelkers et al. (1995)
Aqueous silica	$SiO_{2(aq)}$	-833.41	Oelkers et al. (1995)
Magnesium ion	Mg^{2+}	-453.96	Oelkers et al. (1995)
Pyroaurite	$Mg_3Fe^{3+}(OH)_8(CO_3)_{0.5} \bullet 2.5H_2O$	-3882.60	Rozov et al. (2009)
GR1$(CO_3)^{2-}$	$[Fe_4^{2+}Fe_2^{3+}(OH)_{12}][CO_3 \bullet 2H_2O]$	-4042.79	Drissi et al. (1995)
ISGS berthierine*	$[(Al_{0.976}Fe^{3+}_{0.182}Fe^{2+}_{1.44}Mg_{0.157})(Si_{1.332}Al_{0.668})O_5(OH)_4]$	-3468.31	Blanc et al. (2014)
CCa-2*	$[(Si_{2.633}Al_{1.367})(Al_{1.116}Fe^{3+}_{0.215}Mg_{2.975}Fe^{2+}_{1.712}Ca_{0.011})O_{10}(OH)_8]$	-7607.69	Blanc et al. (2014)
Fe-Chl $(W)_{adj}$	$[(Al_{1.48}Fe^{3+}_{0.33}Fe^{2+}_{2.756}Mg_{1.197})(Si_{2.62}Al_{1.38})O_{10}(OH)_8]$	-7277.81	this study

ISGS Berthierine*, CCa-2* and Fe-Chl$(W)_{adj}$: thermodynamic properties have been modified to eliminate trace components; $\Delta_f G^\circ_{298,1}$ for the oxide species were obtained from Robie and Hemingway (1995).

Figure 1

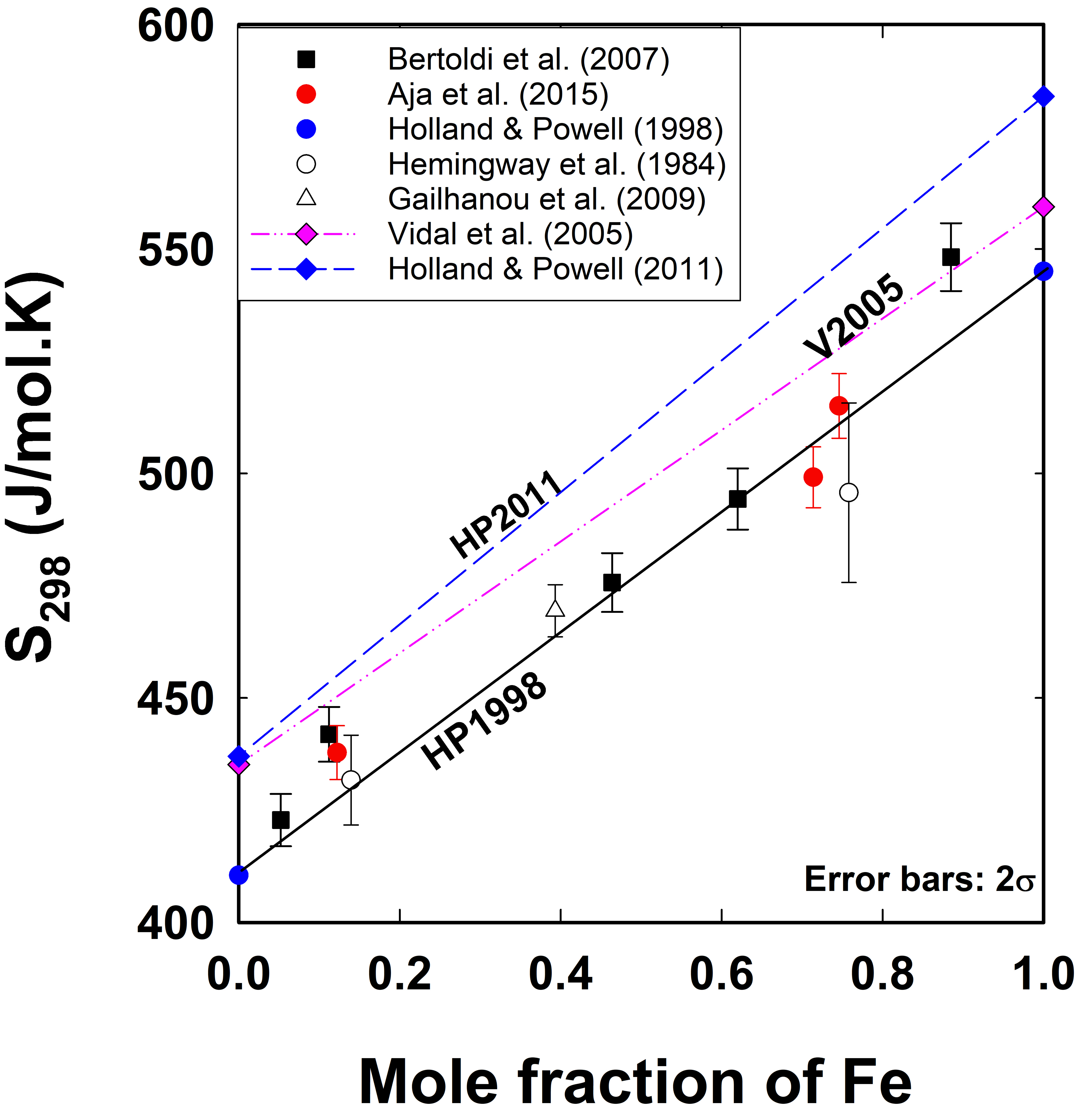

600
550
500
450
400
S_{298} (J/mol.K)
0.0
0.2
0.4
0.6
0.8
1.0
Mole fraction of Fe
■ Bertoldi et al. (2007)
● Aja et al. (2015)
● Holland & Powell (1998)
○ Hemingway et al. (1984)
△ Gailhanou et al. (2009)
◆ Vidal et al. (2005)
◆ Holland & Powell (2011)
HP2011
V2005
HP1998
Error bars: 2σ

Figure 2

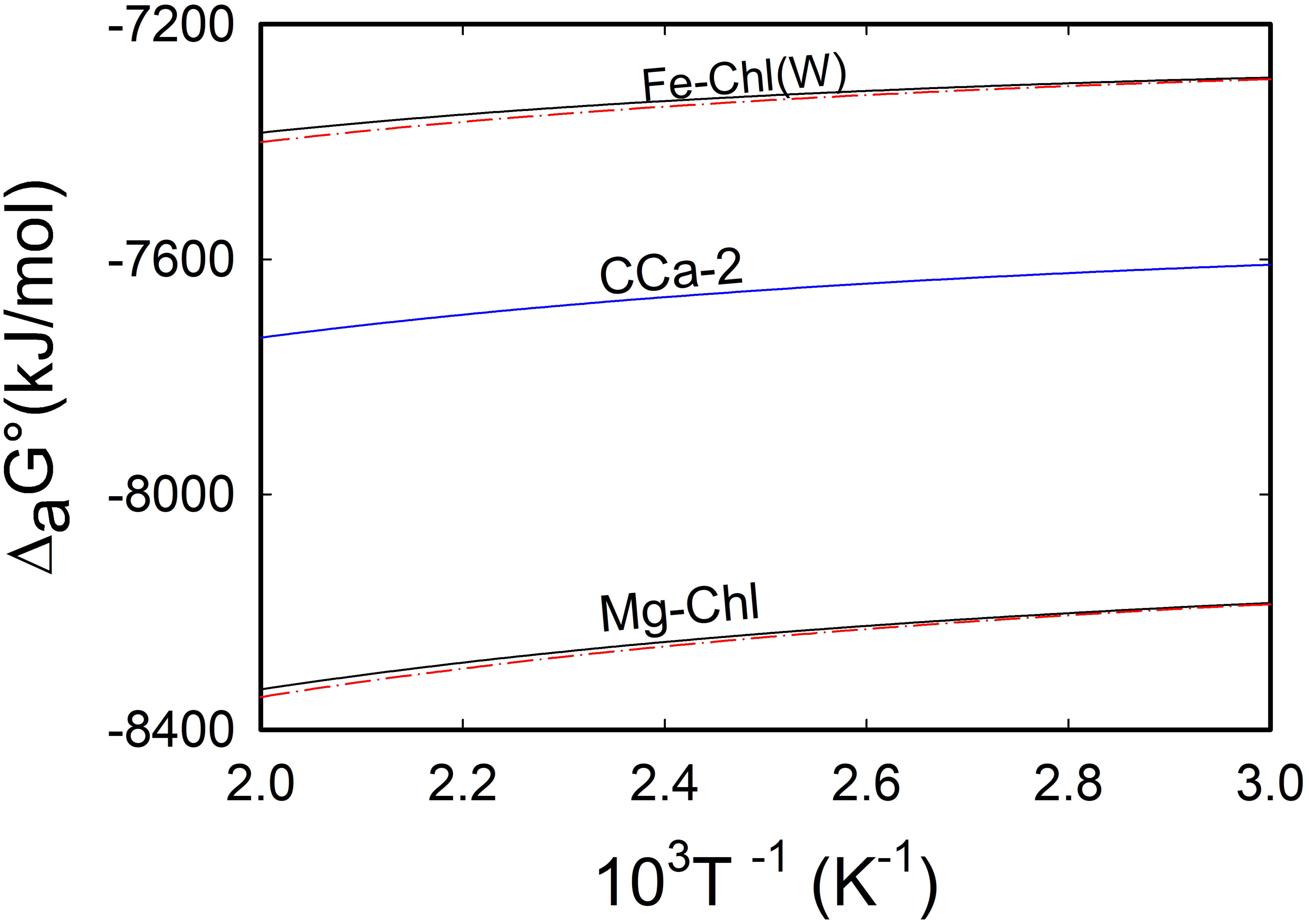
-7200
-7600
-8000
-8400
Fe-Chl(W)
CCa-2
Mg-Chl
2.0
2.2
2.4
2.6
2.8
3.0
$\Delta_a G°$(kJ/mol)
$10^3 T^{-1}$ (K^{-1})

Figure 3a

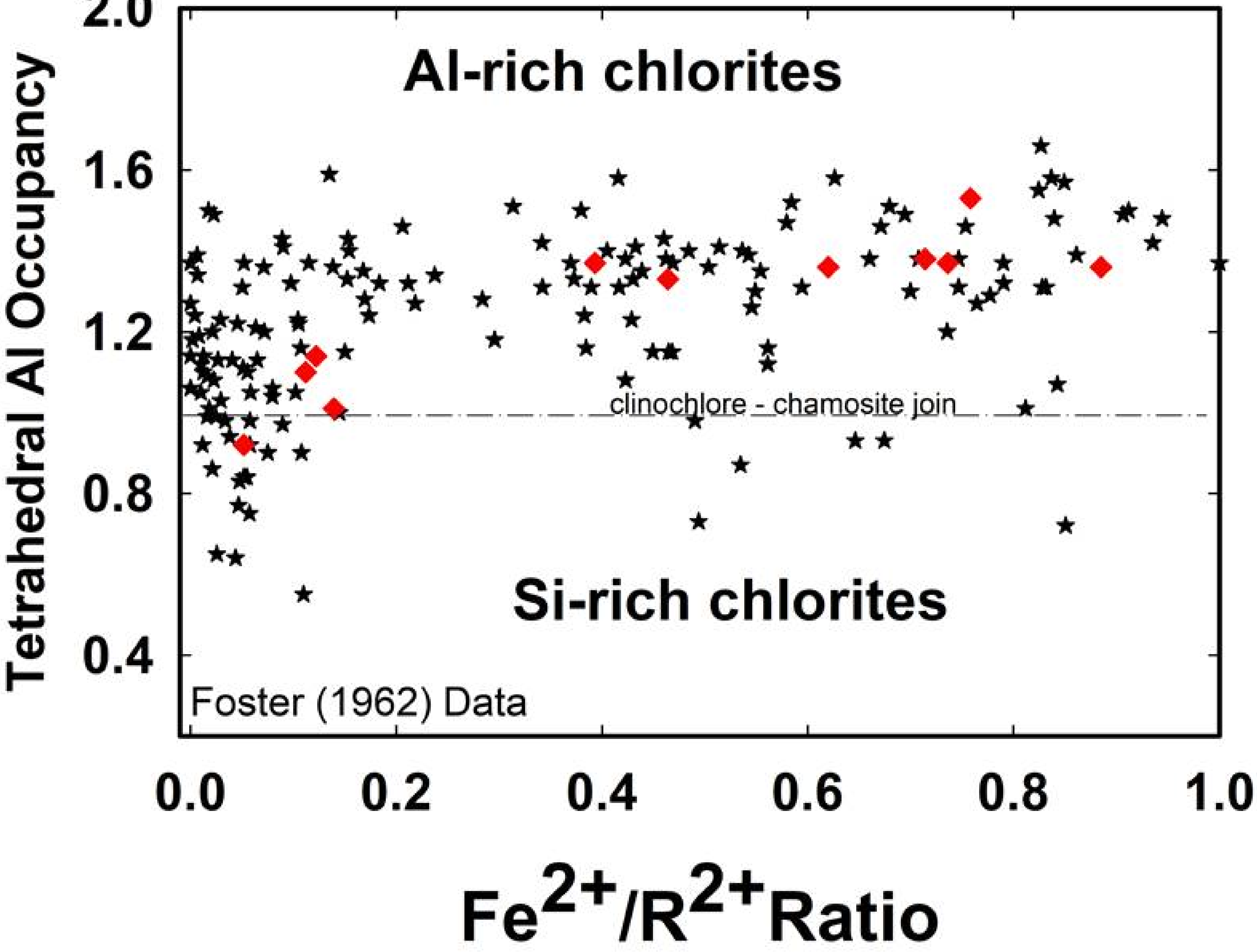
Al-rich chlorites
clinochlore - chamosite join
Si-rich chlorites
Foster (1962) Data
Tetrahedral Al Occupancy
2.0
1.6
1.2
0.8
0.4
0.0
0.2
0.4
0.6
0.8
1.0
Fe^{2+}/R^{2+} Ratio

Figure 3b

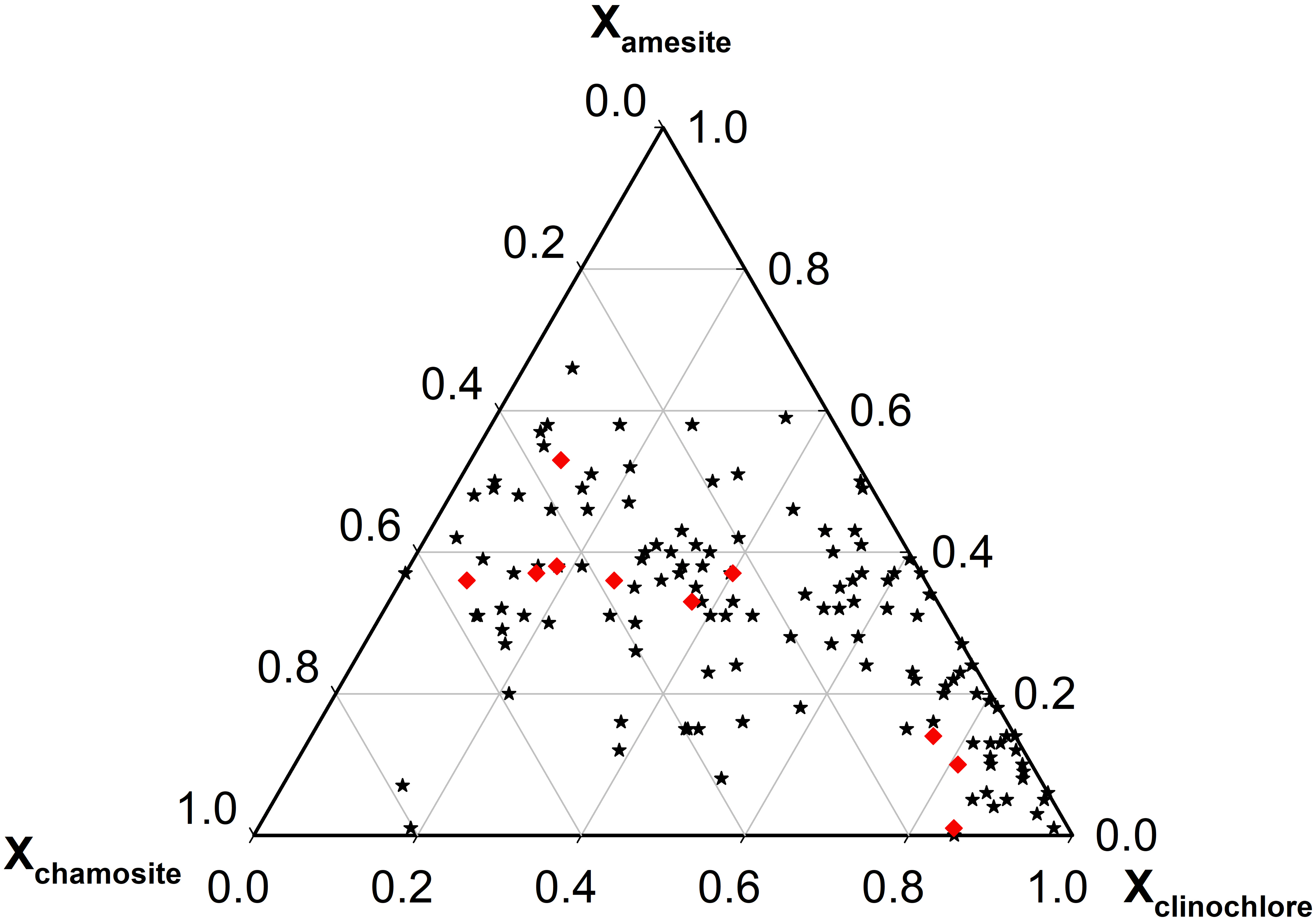
$X_{amesite}$
0.0
0.2
0.4
0.6
0.8
1.0
1.0
0.8
0.6
0.4
0.2
0.0
$X_{chamosite}$
0.0
0.2
0.4
0.6
0.8
1.0
$X_{clinochlore}$

Figure 3c

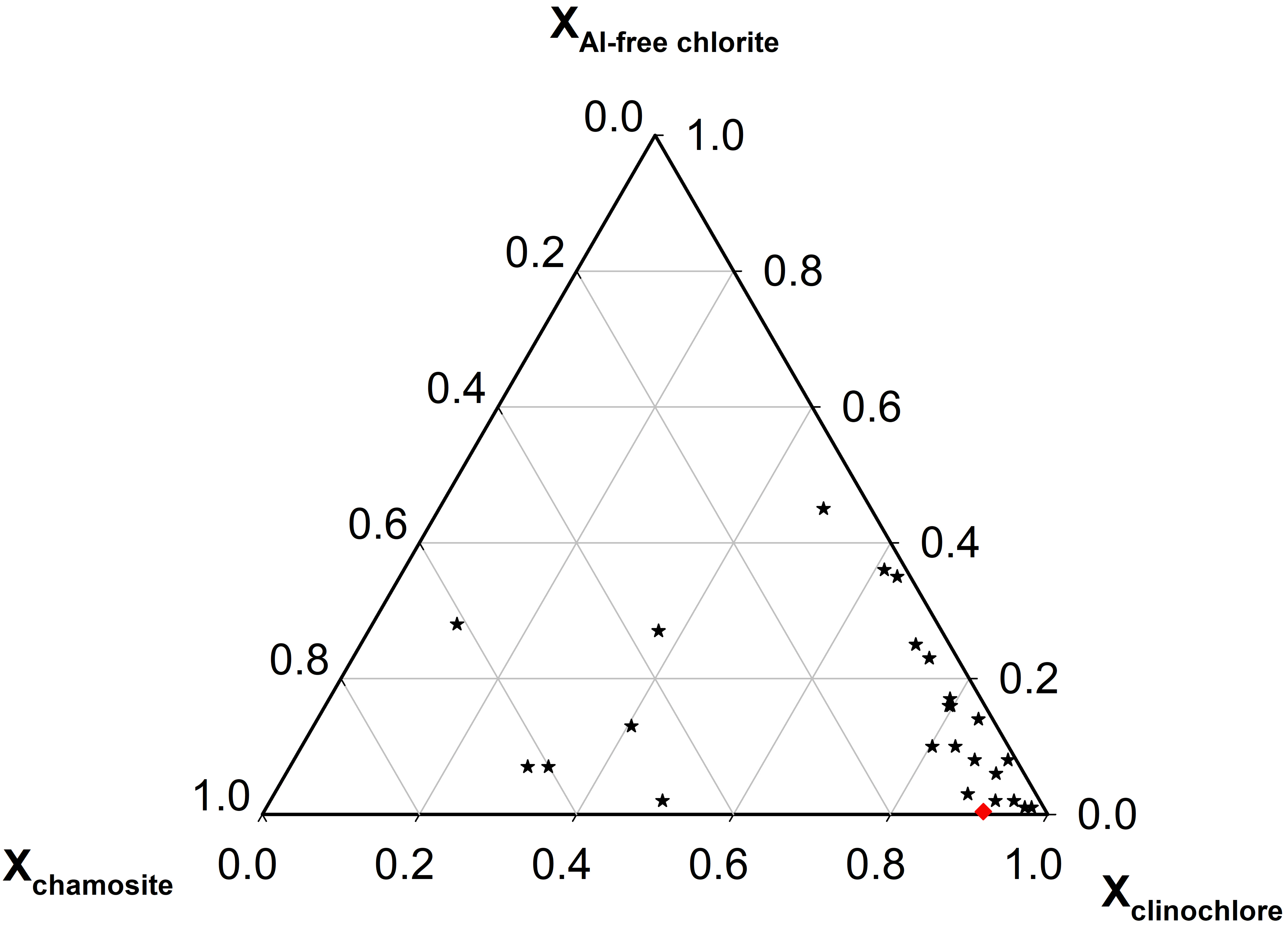
$X_{\text{Al-free chlorite}}$
0.0
0.2
0.4
0.6
0.8
1.0
1.0
0.8
0.6
0.4
0.2
0.0
$X_{\text{chamosite}}$
0.0
0.2
0.4
0.6
0.8
1.0
$X_{\text{clinochlore}}$

Figure 4

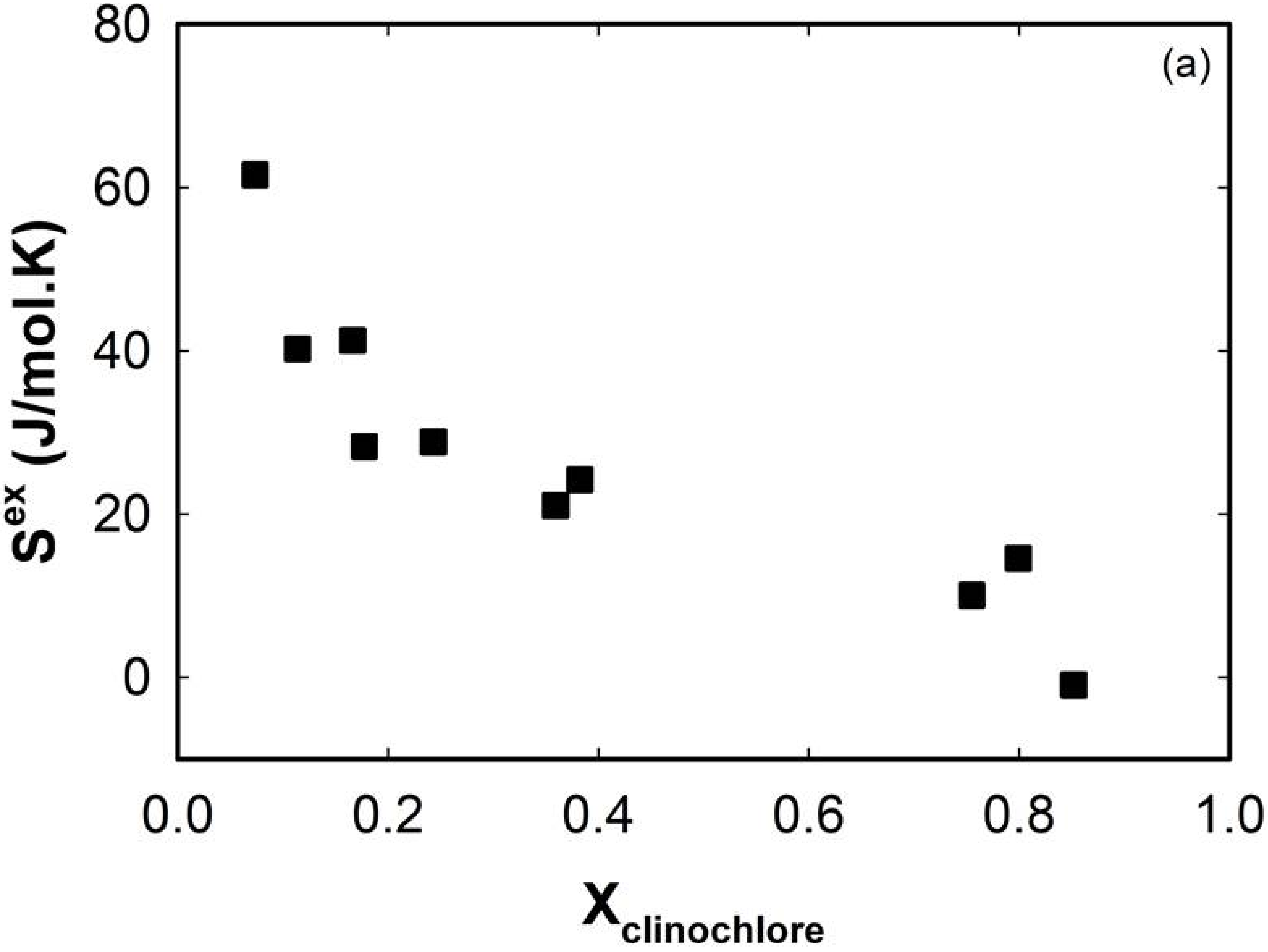

Figure 4

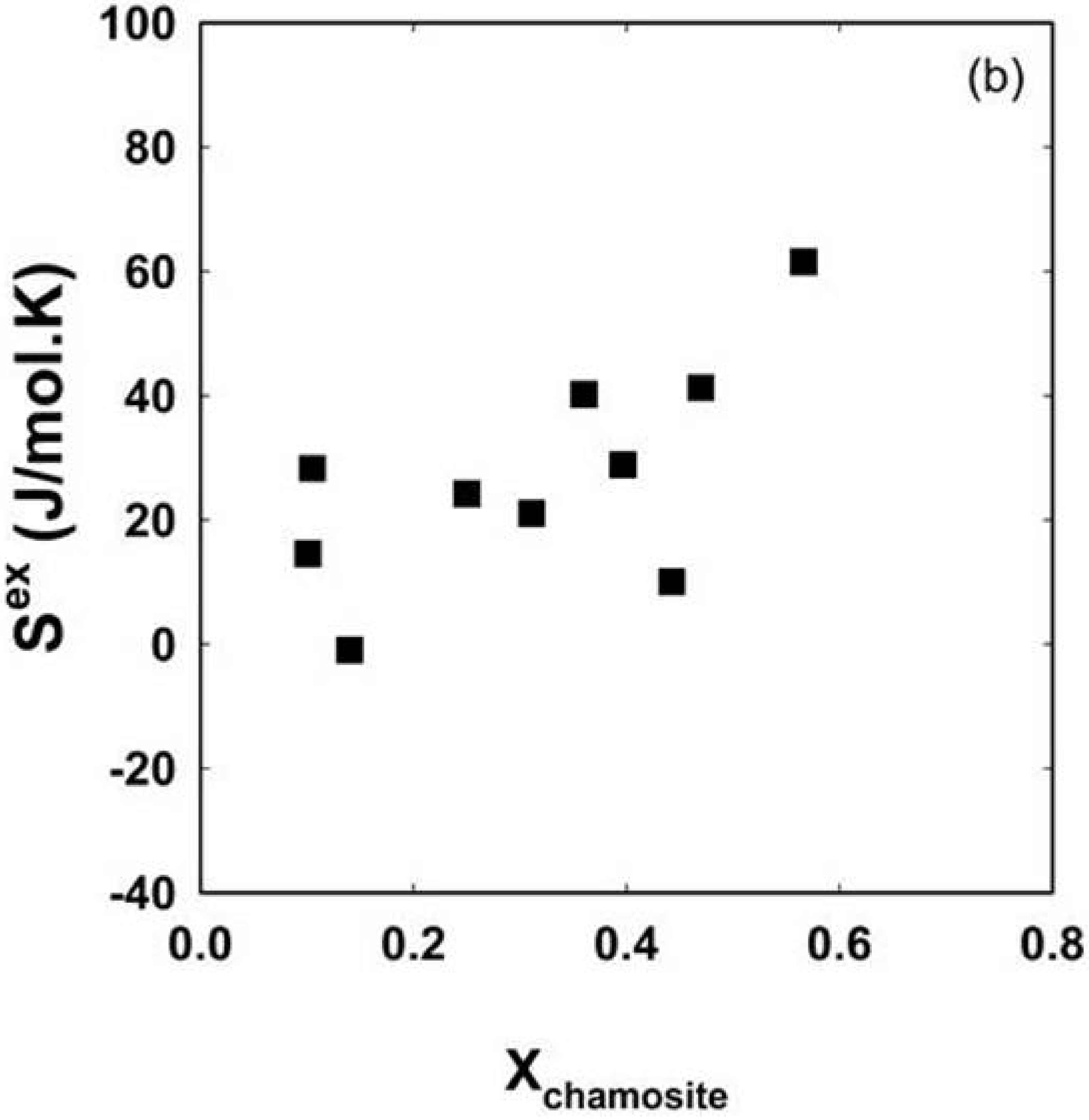

Figure 4

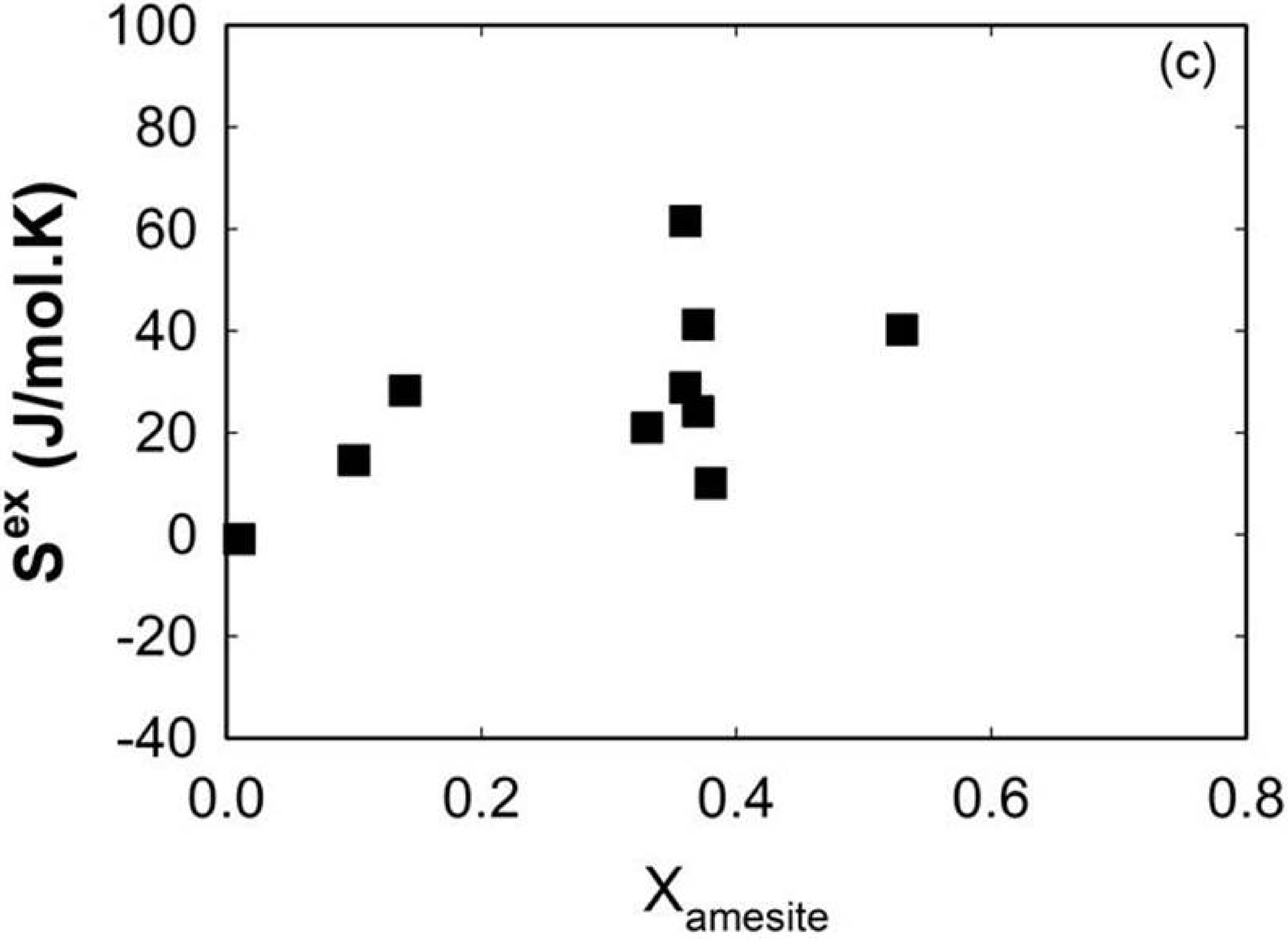

Figure 5

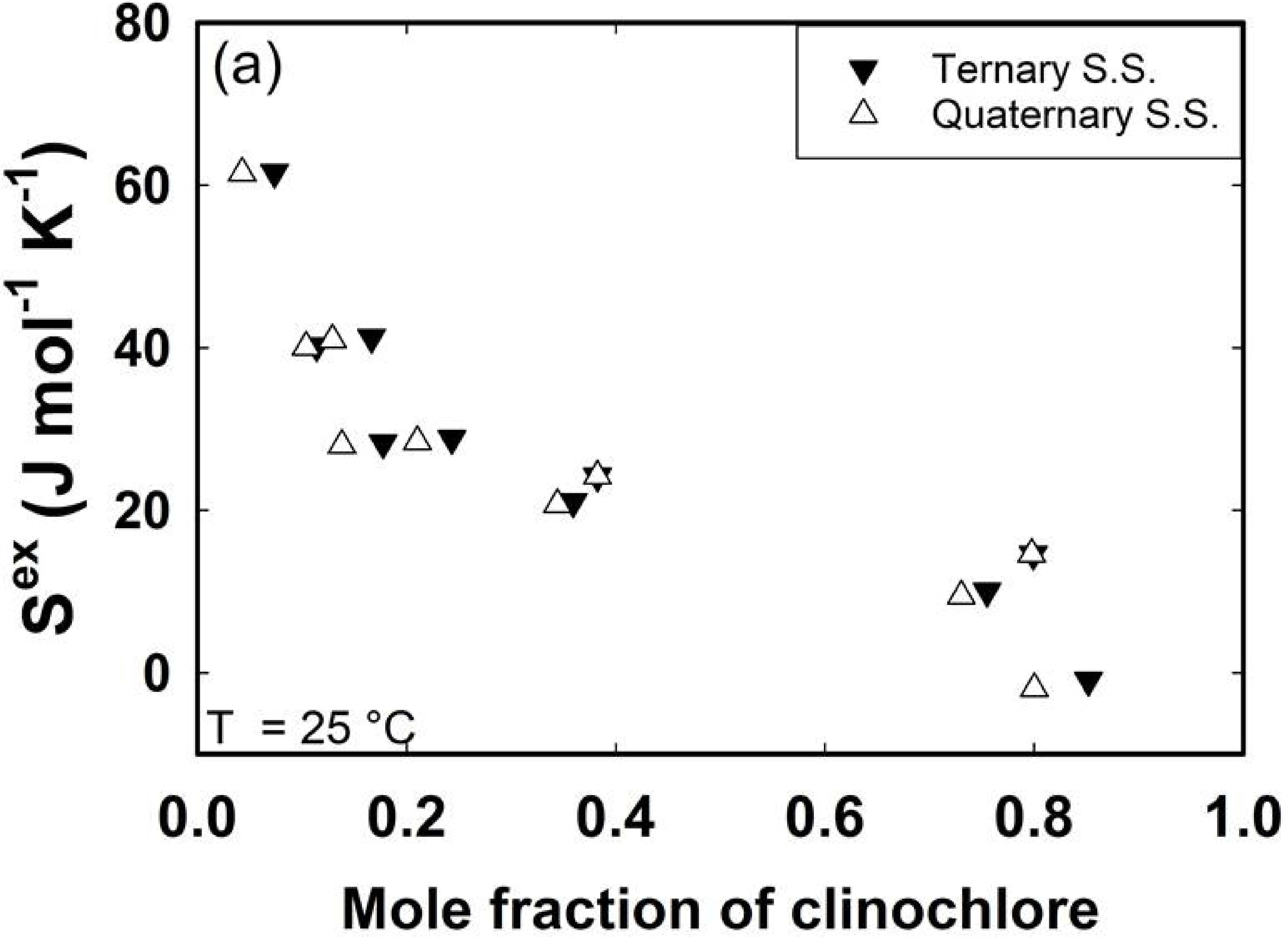
(a)
▼ Ternary S.S.
△ Quaternary S.S.
T = 25 °C
S^{ex} (J mol^{-1} K^{-1})
80
60
40
20
0
0.0
0.2
0.4
0.6
0.8
1.0
Mole fraction of clinochlore

Figure 5

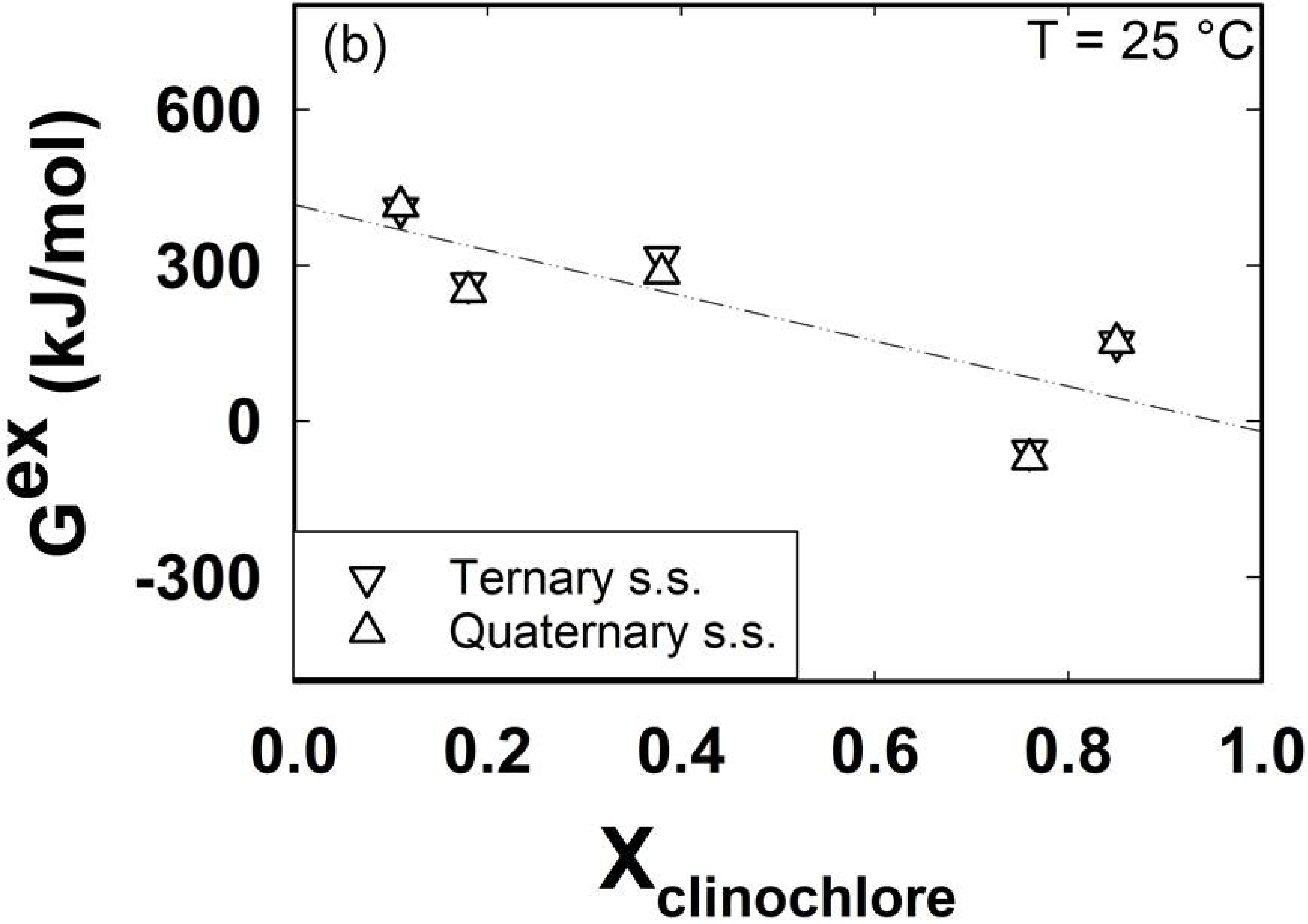
(b)
T = 25 °C
600
300
0
-300
G^ex (kJ/mol)
Ternary s.s.
Quaternary s.s.
0.0
0.2
0.4
0.6
0.8
1.0
X_clinochlore

Figure 6

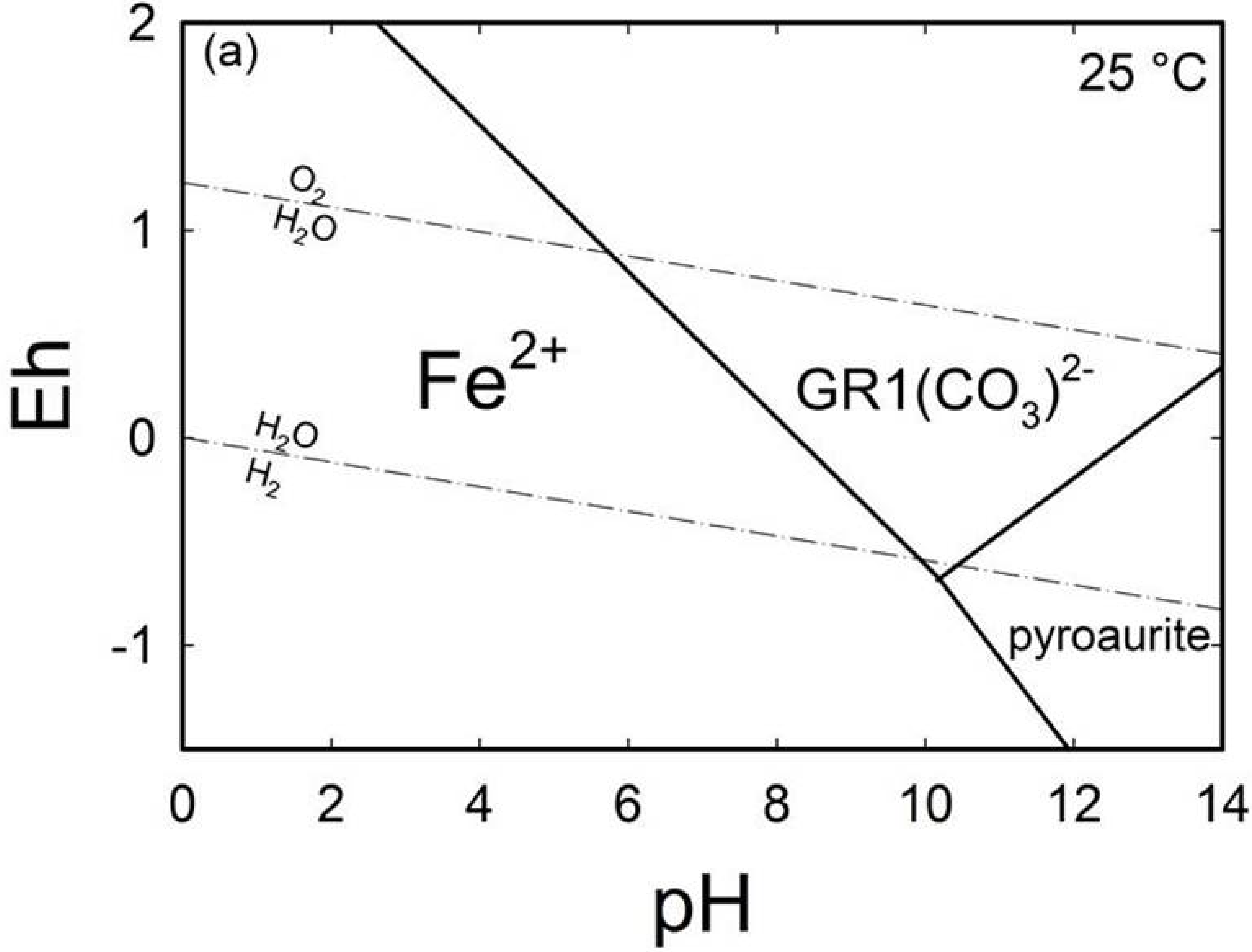
(a)
25 °C
O_2
H_2O
H_2O
H_2
Fe^{2+}
$GR1(CO_3)^{2-}$
pyroaurite
Eh
2
1
0
-1
pH
0
2
4
6
8
10
12
14

Figure 6

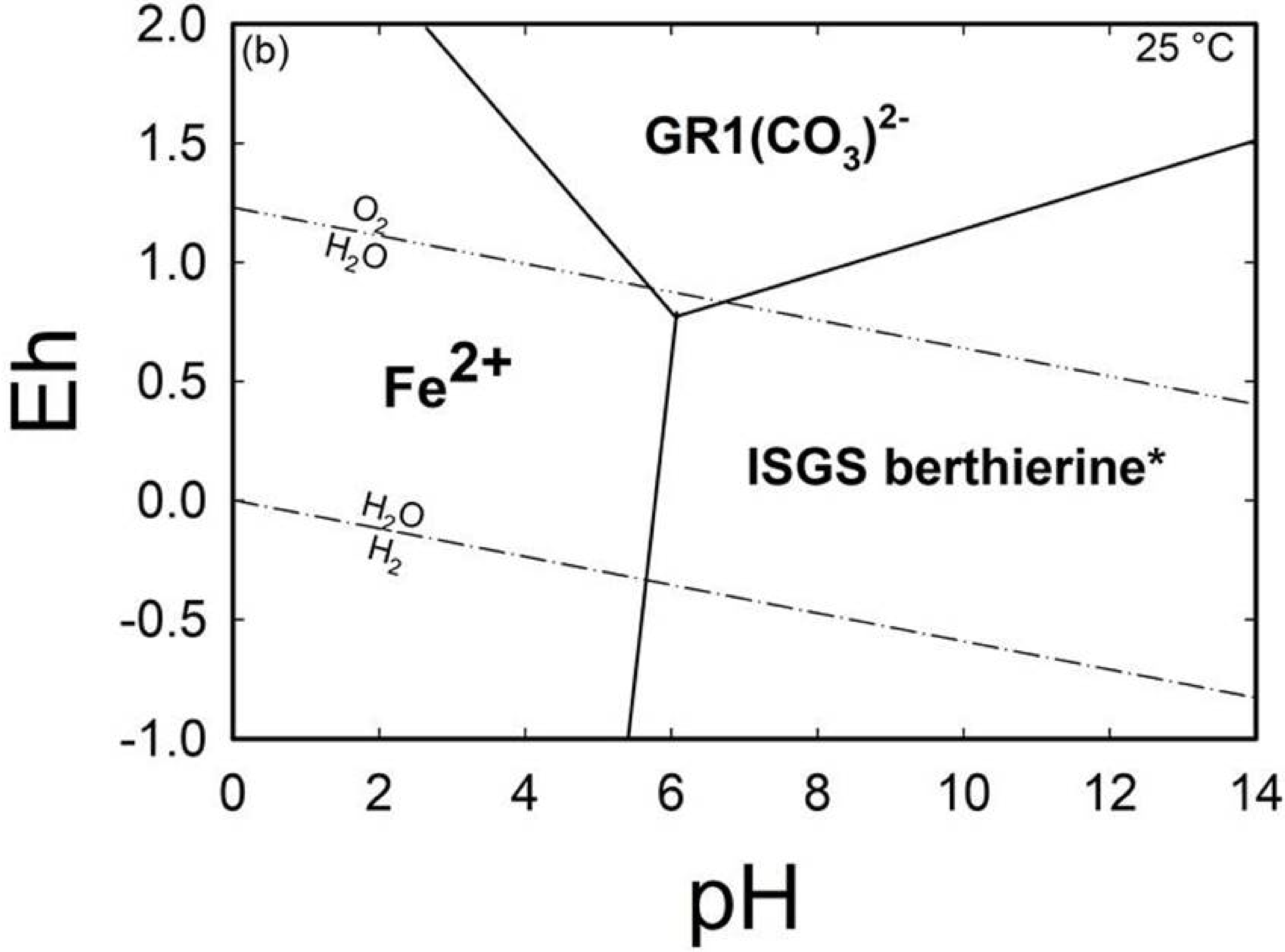
(b)
25 °C
GR1(CO$_3$)$^{2-}$
O_2
H_2O
Fe^{2+}
ISGS berthierine*
H_2O
H_2
Eh
2.0
1.5
1.0
0.5
0.0
-0.5
-1.0
0
2
4
6
8
10
12
14
pH

Figure 6

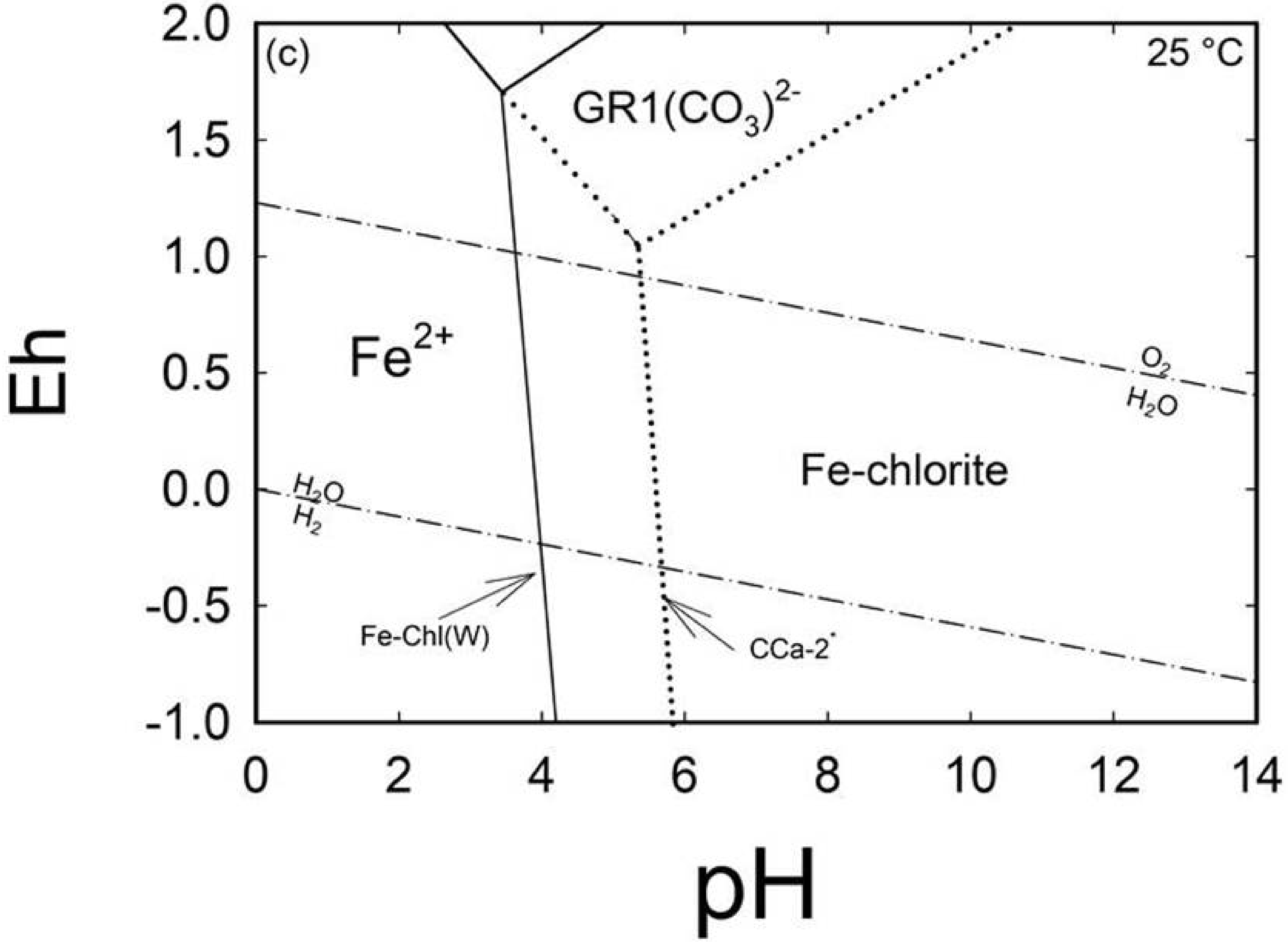
(c)
25 °C
GR1(CO3)2-
Fe2+
Fe-chlorite
O2
H2O
H2O
H2
Fe-Chl(W)
CCa-2*
Eh
2.0
1.5
1.0
0.5
0.0
-0.5
-1.0
pH
0
2
4
6
8
10
12
14